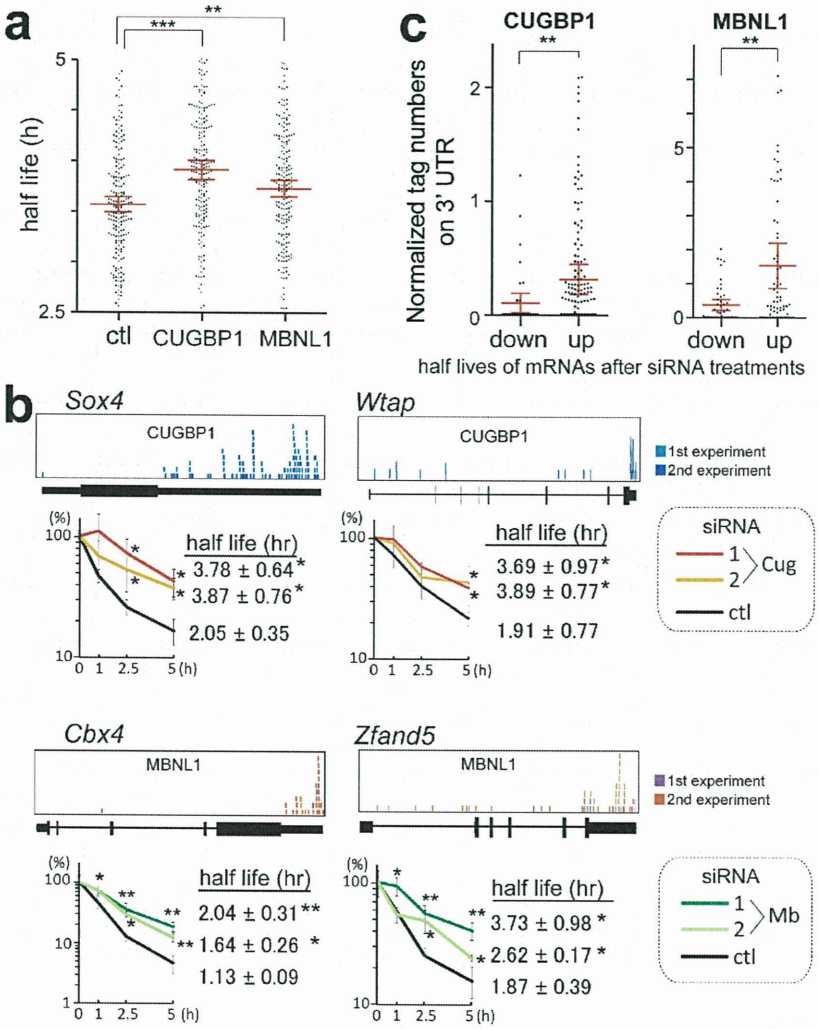

Figure 5 | Global analysis of mRNA decay by expression array of C2C12 cells treated with CUGBP1/MBNL1 siRNA. (a) Half-lives of mRNAs in C2C12 cells with the indicated siRNAs. Red lines represent means and 95% confidence intervals. ** $p < 0.01$ and *** $p < 0.001$. (b) Real-time RT-PCR analysis of the stability of four representative endogenous mRNAs, which were detected by expression arrays. CLIP-tag distributions are shown above each gene structure. C2C12 cells were treated with either control (ctl), CUGBP1 (Cug), or MBNL1 (Mb) siRNA. Actinomycin D was added to the medium to stop transcription at time 0. Temporal profiles of decay of the indicated genes were analyzed by real-time RT-PCR and are normalized for *Gapdh* mRNA levels. All experiments were triplicated, and the mean and s.d. are indicated (* $p < 0.05$ and ** $p < 0.01$). (c) Tag counts in the 3′ UTR of each gene are plotted in two categories of prolonging (up) and shortening (down) of half-lives after MBNL1 and CUGBP1 siRNAs. Red lines represent means and 95% confidence intervals. ** $p < 0.01$. Tag counts were normalized by the gene expression level at 0 h of cells treated with control siRNA.

Table 1 | The five most frequent Gene Ontology terms of mRNAs that are bound by CUGBP1 and MBNL1 to the 3′ UTR

CLIP data	GO ID	Term	P Value
CUGBP1	GO:0008092	cytoskeletal protein binding	1.58E-06
	GO:0003723	RNA binding	1.40E-04
	GO:0008134	transcription factor binding	9.65E-04
	GO:0051082	unfolded protein binding	0.003184
	GO:0019904	protein domain specific binding	0.006603
MBNL1	GO:0008092	cytoskeletal protein binding	7.31E-20
	GO:0008134	transcription factor binding	2.20E-08
	GO:0003723	RNA binding	0.001893
	GO:0019899	enzyme binding	0.002046
	GO:0032553	ribonucleotide binding	0.004210

We utilized the mRNAs that have more than 8-fold coverage of CLIP tags in their 3′UTR for the analysis by DAVID[53,54].

PITX2 is a homeobox transcription factor that regulates left-right asymmetric morphogenesis[37,38] and it is also deeply implicated in myogenesis during mouse embryonic development[39–41]. We found that the decay of *Pitx2* mRNA is prolonged by knocking down MBNL1, but not CUGBP1 in undifferentiated C2C12 cells (Fig. 6b and c). This is consistent with the fact that *Pitx2* harbors a much higher number of MBNL1-CLIP tags than that of CUGBP1-CLIP tags in the 3′ UTR (Fig. 6a). We also observed that down regulation of both CUGBP1 and MBNL1 decreases the decay of *Myod1* and *Mbnl2* mRNA, but not that of *Gapdh* mRNA (Supplementary Fig. S8). Similarly, down regulation of CUGBP1 decreases the decay of other myogenic transcription factors such as *Myog* and *Mef2a* mRNAs, and also of *Cugbp2* (Supplementary Fig. S9). Furthermore, knockdown of CUGBP1 and MBNL1 prolongs decay of *Mbnl1* and *Cugbp1* mRNAs, respectively, suggesting a mechanism for cross-regulation of expression of MBNL1, CUGBP1, and their family proteins (Supplementary Fig. S8).

To analyze more directly the role of MBNL1 binding to the 3′ UTR in regulation of mRNA decay, we examined the mRNA stability of firefly luciferase fused with the 3′ UTR of *Pitx2* (Fig. 6a). There are 11 YGCY motifs in the 3′ UTR of *Pitx2*, and 4 of the 11 motifs have MBNL1-CLIP tags. We introduced artificial mutations in these 4 motifs to prevent binding of MBNL1 (Fig. 6a). Consistent with the proposed role for MBNL1 in mRNA decay, we observe that disruption of the MBNL1-binding motifs in the *Pitx2*-3′ UTR abolished responsiveness to MBNL1 knockdown (Fig. 6d). Furthermore, immunoblots demonstrated that MBNL1-knockdown enhanced expression of endogenous PITX2 in C2C12 cells (Fig. 6e). These data suggest that MBNL1 promotes decay of *Pitx2* mRNA and thereby represses expression of the PITX2 protein.

Taken together, all of our data are consistent with a model where CUGBP1 and MBNL1 facilitate mRNA decay through binding to the 3′ UTR of target genes.

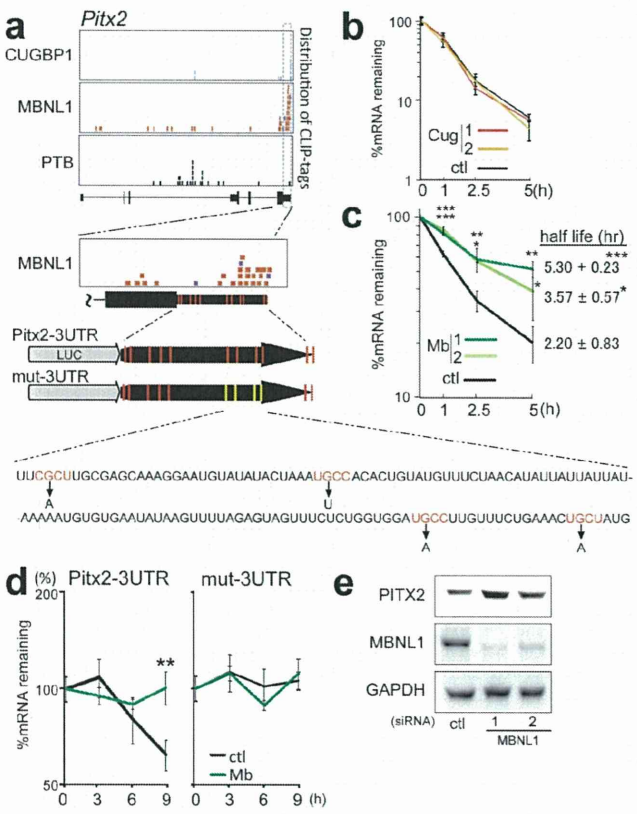

Figure 6 | MBNL1 binds to 3′ UTR of *Pitx2* and facilitates decay of *Pitx2* mRNA. (a) Distributions of MBNL1 CLIP-tags in the *Pitx2*-gene structure, and schemes of luciferase reporter plasmids harboring wild-type (*Pitx2*-3UTR) and mutated (mut-3UTR) 3′ UTRs of *Pitx2*. Red bars indicate locations of native YGCY motifs and yellow bars indicate those of mutated YGCY motifs. Individual mutations disrupting YGCY motifs are shown at the bottom. We introduced U at the 2nd YGCY motif to prevent formation of AU and AC repeats, which constitute a potential binding site of Hu proteins and hnRNP L, respectively. (b and c) Decay of endogenous *Pitx2* mRNA by siRNA-mediated knockdown of CUGBP1 (b) and MBNL1 (c). C2C12 cells were treated with either control (ctl), CUGBP1 (Cug) or MBNL1 (Mb) siRNA. Actinomycin D was added to the medium to stop transcription at time 0. Temporal profiles of decay of the indicated genes were analyzed by real-time RT-PCR and were normalized for *Gapdh* mRNA levels. All experiments were triplicated, and the mean and s.d. are indicated (* $p < 0.05$; ** $p < 0.01$; *** $p < 0.001$). (d) Decay of luciferase mRNA in the Pitx2-3UTR and mut-3UTR constructs after either control (ctl) or MBNL1 (Mb) siRNA in TetON-C2C12 cells. Culture medium was replaced by medium without doxycycline to stop transcription at time 0. Temporal profiles of luciferase mRNA decay are quantified by real-time RT-PCR and are normalized for *Gapdh* mRNA levels. All experiments were triplicated, and the mean and s.d. are indicated (** $p < 0.01$). (e) Immunoblot of PITX2 in undifferentiated C2C12 cells at 48 hrs after transfection of MBNL1 siRNA.

Discussion

CUGBP1 and MBNL1 are developmentally regulated RNA-binding proteins that are causally associated with myotonic dystrophy type 1. In this study, we show that both CUGBP1 and MBNL1 preferentially bind to 3′ UTRs and destabilize the bound mRNAs. In particular, we show that CUGBP1 and MBNL1 destabilize myogenic differentiation factors and RNA-binding proteins. In addition, our results confirm and significantly expand the current knowledge of the splicing-regulatory effects of CUGBP1 and MBNL1. Taken together, the data from the present study indicates that CUGBP1 and MBNL1 are closely related and cross regulate alternative splicing and mRNA decay.

MBNL1 binding to 3′ UTRs has not been previously reported. We show for the first time that MBNL1 binds to 3′ UTRs and promotes mRNA decay in both artificial constructs and in endogenous genes. We also demonstrate by expression arrays that both CUGBP1 and MBNL1 facilitate mRNA decay by binding to 3′ UTRs. The present study demonstrates global *in vivo* interactions between CUGBP1 and 3′ UTRs and reveals that CUGBP1 also preferentially binds to 3′ UTR rather than exons/introns. We provide *in vivo* evidence that CUGBP1 facilitates mRNA decay of a broad spectrum of genes in addition to the previously reported genes[25–27,42–44].

Interestingly, we find that MBNL1 promotes decay of *Cugbp1* mRNA and that CUGBP1 promotes decay of *Mbnl1* mRNA, and that this is associated with corresponding changes at the protein level during differentiation of C2C12 cells (Supplementary Fig. S4b). This may suggest that expression of CUGBP1 and MBNL1 are mutually regulated in myogenic differentiation. Kuyumcu-Martinez and colleagues report that expanded CUG repeats of *DMPK* through an unknown mechanism leads to phosphorylation and thereby to stabilization of CUGBP1 in DM1 myoblasts[10]. Our studies additionally suggest that loss of MBNL1 in DM1 could lead to decreased decay of *CUGBP1* mRNA and hence to further increase of CUGBP1 activity. Although CUGBP1 is not upregulated in adult MBNL1-knockout mice, this mechanism could lead to increased misregulation of splicing and decay of the mRNAs of target genes in embryonic development that culminates in the DM1 phenotype.

We find that binding sites for CUGBP1 and MBNL1 are enriched around alternative cassette exons (Fig. 2a). The binding sites for CUGBP1 are prominent in adjacent intronic regions flanking alternative exons. Our functional analysis reveals that binding of CUGBP1 to the upstream intron facilitates exon skipping, whereas

binding to the downstream intron enhances exon inclusion (Fig. 2b). Interestingly, similar regulation of alternative splicing has been observed for NOVA, FOX2 and PTB[30,45,46], indicating the presence of a common underlying mechanism shared by these proteins.

In contrast to CUGBP1, MBNL1 tags are also enriched in coding exons. Until now, splicing *cis*-elements of MBNL1 have been mapped exclusively to introns, and no exonic *cis*-element has been reported to our knowledge[20,23,34,47,48]. Although MBNL1 preferentially binds to exons, MBNL1 binding to introns is enriched at alternative rather than constitutive splice sites (Fig. 2a. This enrichment is diffusely distributed throughout regions harboring 500 nt upstream or downstream of alternative exons, in contrast to the prominent intronic peaks observed for CUGBP1 tags. This could suggest that MBNL1 needs to bind simultaneously to the target exon and adjacent introns to regulate splicing. Functional analysis of MBNL1 reveals that binding of MBNL1 close to the 3′ end of the downstream intron facilitates exon skipping, whereas no characteristic binding pattern is observed for exons included in response to MBNL1 (Fig. 2c). PTB has also been reported to regulate alternative splicing through binding close to the 3′ end of the downstream intron[36]. In contrast to MBNL1, however, binding of PTB to this region promotes exon inclusion. We similarly find binding of PTB to this region in our HITS-CLIP data in MBNL1-regulated exons (Supplementary Fig. S7d). Interestingly, the MBNL1-binding motif is enriched in PTB-regulated exons[46]. MBNL1 may thus compete for binding with other splicing factors like PTB and regulate alternative splicing events.

Post-transcriptional gene expression regulation is crucial to achieve precise developmental and tissue-specific control of cellular processes. Our studies reveal that CUGBP1 and MBNL1 preferentially bind to the 3′ UTRs of mRNAs encoding RNA-binding proteins and transcription factors, which can regulate cell development. During development of murine skeletal muscles, the nuclear level of MBNL1 increases, while that of CUGBP1 decreases[9,12]. Genes with mRNAs that can be bound both by CUGBP1 and MBNL1 are likely to be down-regulated by CUGBP1 in undifferentiated cells. If these genes need to be tightly down-regulated also in differentiated cells, MBNL1 can substitute for CUGBP1 in order to achieve continued destabilization of the target mRNA. We conclude that finely-tuned expression of CUGBP1 and MBNL1 may be important regulators of myogenic differentiation through precise regulation of both alternative splicing and mRNA stability.

Methods

Antibodies. Antibodies to CUGBP1 (3B1), MHC (H300), myogenin (M225) and PTB (N20) were purchased from Santa Cruz Biotechnology. Anti-GAPDH pAb was purchased from Sigma. Anti-PITX2 pAb was purchased from Abcam. Anti-MBNL1 rabbit serum (A2764) was a kind gift of Dr. Charles A. Thornton at University of Rochester. The specificity of antibodies against CUG BP1 and MBNL1 is supported by the data in previous reports 2,3 and also by our siRNA experiments (Supplementary Fig. S1).

Cell culture. Detailed methods are included in the Supplementary Information.

HITS-CLIP. C2C12 cells were UV-irradiated at 400 mJ and CLIP was performed as previously described[49]. High-throughput 36-bp single-end and 40-bp single-end sequencing was performed using an Illumina Genome Analyzer II. All HITS-CLIP data were registered in ArrayExpress with an accession number E-MTAB-414 and in ENA with an accession number ERP000789. Detailed information is provided in the Supplementary Information.

Bioinformatics analysis. Illumina reads were first prepared by removing the 4-bp tag and filtering sequences composed primarily of Illumina adapter. The resulting reads were mapped to the mouse genome (NCBI Build 37.1/mm9) with default parameters using the BWA[50] mapping software. To extract consensus motifs from the mapped reads, we considered only uniquely aligned reads and first removed duplicate reads to avoid potential PCR-mediated deviations in addition to bias from very highly expressed transcripts. We then extended the reads to 110 nt, the expected mean of the CLIP fragments and used the SeqMonk software (www.bioinformatics.bbsrc.ac.uk/projects/seqmonk) to identify binding regions by using the program's built-in peak detection algorithm. Peaks were scored using both a reads per peak scoring scheme and a maximum depth scoring scheme (effectively the height of the peak) in order to filter out peaks. For the identification of CUGBP1- and MBNL1-binding regions, we used PTB as a negative control and removed peaks present in the PTB dataset as well. We then selected CUGBP1 peaks that were present in the two independent CUGBP1 CLIP experiments and MBNL1 peaks that were similarly corroborated by the two MBNL1 experiments. PTB binding regions were identified by removing peaks that were present in either of the four CUGBP1 and MBNL1 experiments. Finally, we restricted the set of binding regions to only those spanning 70–150 bp since this was the fragment length used in the CLIP experiments. We analyzed each dataset using a motif analysis tool, MEME[31], using a background Markov model based on the entire mouse genome.

We analyzed the mapped Illumina reads and binding regions and mapped them to UCSC knownGene annotations[51] of the mouse genome (NCBI Build 37.1/mm9) by writing and running Perl and Excel VBA programs, as well as by running BEDTools utilities[52]. Normalized complexity maps of CUGBP1/MBNL1/PTB-RNA interactions were generated as previously described[30]. For the control, normalized complexity map was similarly generated by analyzing 100 sets of 15 to 50 constitutive exons that were randomly selected from 118,969 constitutive exons in mm9. To identify enriched Gene Ontology terms, we used the Database for Annotation, Visualization and Integrated Discovery (DAVID 6.7)[53,54].

Construction of plasmids. To construct luciferase reporter vectors with the 3′ UTR of *Gapdh* and *Pitx2*, 3′ UTRs of these genes were amplified by PCR. Amplified DNA was ligated into the *Xba*I and *Bam*HI sites of the pGL3-promoter vector (Promega) to substitute for the 3′ UTR of the firefly luciferase gene. DNA fragments harboring GT and CTG repeats were amplified by self-priming PCR using primers terminating in a *Xba*I site, and ligated into the *Xba*I site to make the pGL3P-*Gapdh*-3′ UTR.

To construct tet-responsive luciferase constructs, the tet-responsive promoter region was excised from pTRE-Tight vector (Clontech) with *Xho*I-*Hin*dIII site and cloned into the *Xho*I-*Hin*dIII site of the pGL3-promoter vector with the 3′ UTR of *Gapdh* and *Pitx2*. To introduce mutations in 3′ UTR of *Pitx2* in the luciferase construct, we used the QuikChange site-directed mutagenesis kit (Stratagene).

To construct expression vectors for MBNL1 and CUGBP1, the human MBNL1 cDNA and human CUGBP1 cDNA (Open Biosystems) were subcloned into the mammalian bidirectional expression vector pBI-CMV2 (Clontech), which should constitutively expresses the insert and AcGFP1.

RNA interference and transfection. The siRNA duplexes against CUGBP1 and MBNL1 were synthesized by Sigma. The sense sequences of the siRNAs were as follows: Cugbp1-1, 5′-GCUUUGGUUUUGUAAGUUA-3′; Cugbp1-2, 5′-GGCUUAAAGUGCAGCUCAA-3′; Mbnl1-1, 5′-CACUGGAAGUAUGUAGAGA-3′; and Mbnl1-2, 5′-GCACAAUGAUUGAUACCAA-3′. We purchased the AllStar Negative Control siRNA (1027281) from Qiagen. C2C12 cells were seeded on 24-well plates, and transfected with siRNA using Lipofectamine 2000 (Invitrogen) according to the manufacturer's instructions. Tet-off advanced HEK293 cells were seeded on 96-well plates, and were transfected with luciferase reporter gene constructs using FuGENE 6 (Roche) according to the manufacturer's instructions. At 48 hrs after transfection, cells were either harvested for RNA extraction or processed for isolation of total proteins or nuclear extracts.

RT-PCR for splicing analysis. Total RNA was extracted using Trizol (Invitrogen) according to the manufacturer's instructions. cDNA was synthesized using an oligo-dT primer and ReverTra Ace (Toyobo), and PCR amplifications were performed using GoTaq (Promega) for 30–35 cycles. Sequences of the primers used for PCR are listed in the Supplementary Table S3. The intensities of PCR-amplified spliced products were quantified with the ImageJ 1.42q software (NIH). We then calculated a percentage of exon inclusion (% inclusion) as the ratio of the intensity of the upper band divided by the sum of intensities of all the bands.

Real-time RT-PCR for RNA stability analysis. Total RNA was extracted using RNeasy mini kit (Qiagen) or CellAmp Direct RNA Prep Kit (Takara) according to the manufacturer's instructions. cDNA was synthesized as described above and real-time PCR was performed using the Mx3005P QPCR System (Stratagene) and the SYBR Premix Ex Taq II (Takara). Sequences of the primers used for PCR are listed in Supplementary Table S4.

Microarray analysis. Total RNA was extracted using the RNeasy mini kit according to the manufacturer's instructions. We synthesized and labeled cDNA fragments from 100 ng of total RNA using the GeneChip WT cDNA Synthesis Kit (Ambion). The labeled cDNAs were hybrized to the Affymetrix Mouse Exon 1.0 ST Arrays for splicing analysis or the Affymetrix Mouse Gene 1.0 ST Arrays for analyzing temporal profiles of expression of CUGBP1/MBNL1-targeted genes following the manufacturer's protocols. The robust multichip analysis (RMA) algorithm was used to normalize the array signals across chips with the Affymetrix Expression Console software 1.1.2. All microarray data were uploaded to the Gene Expression Omnibus database (accession numbers, GSE29990 for exon arrays and GSE27583 for expression arrays).

Western blotting. For preparation of total cell lysates, cells were lysed in buffer A (10 mM HEPES pH 7.8, 10 mM KCl, 0.1 mM EDTA, 1 mM DTT, 2 μg/ml Aprotinin, 0.5 mM PMSF, 0.1% NP-40) and incubate on ice for 20 min. After sonication, samples were centrifuged (15,000 rpm, 5 min) and the supernatants were stored at −80°C for further experiments. For preparation of nuclear cell lysates, cells were suspended in 400 μl of buffer A. Nuclei were pelleted, and the cytoplasmic

proteins were carefully removed. The nuclei were then resuspended in buffer C (50 mM HEPES pH 7.8, 420 mM KCl, 0.1 mM EDTA, 5 mM $MgCl_2$, 2% Glycerol, 1 mM DTT, 2 μg/ml Aprotinin, and 0.5 mM PMSF). After vortexing and stirring for 20 min at 4°C, the samples were centrifuged, and the supernatants were stored at −80°C. Samples were analyzed on a 10% SDS polyacrylamide gel, and the proteins were transferred to Immobilon polyvinylidene difluoride membranes (Millipore). Membranes were blocked with 1% BSA in Tris-buffered saline containing 0.05% Tween20 (TBST) for 1 hr, incubated for 1 hr with primary antibodies in TBST, washed three times with TBST, and incubated for 1 hr with horseradish peroxidase-conjugated anti-mouse or -rabbit immunoglobulin (GE) diluted 1 : 5,000 in TBST. After three washes in TBST, the blot was developed with the enhanced chemiluminescence system (GE) according to the manufacturer's instructions.

Luciferase assay. HEK293 cells seeded on a 96 well plate were transfected with 10 ng of pGL3P-*Gapdh*-3′ UTR with or without GT and CTG repeats, 5 ng of pRL/SV40 (Promega), and 40 ng of pBI-CMV2-based CUGBP1 or MBNL1 expression vector using FuGENE 6. At 48 hrs after the transfection, the luciferase activity was measured using the Dual-Luciferase Reporter Assay System (Promega) according to the manufacturer's instructions.

1. Licatalosi, D. D. & Darnell, R. B. RNA processing and its regulation: global insights into biological networks. *Nat Rev Genet* **11**, 75–87 (2010).
2. Wang, G. S. & Cooper, T. A. Splicing in disease: disruption of the splicing code and the decoding machinery. *Nat Rev Genet* **8**, 749–61 (2007).
3. Brook, J. D. *et al.* Molecular basis of myotonic dystrophy: expansion of a trinucleotide (CTG) repeat at the 3′ end of a transcript encoding a protein kinase family member. *Cell* **68**, 799–808 (1992).
4. Day, J. W. & Ranum, L. P. RNA pathogenesis of the myotonic dystrophies. *Neuromuscul Disord* **15**, 5–16 (2005).
5. Larkin, K. & Fardaei, M. Myotonic dystrophy—a multigene disorder. *Brain Res Bull* **56**, 389–95 (2001).
6. Lee, J. E. & Cooper, T. A. Pathogenic mechanisms of myotonic dystrophy. *Biochem Soc Trans* **37**, 1281–6 (2009).
7. Turner, C. & Hilton-Jones, D. The myotonic dystrophies: diagnosis and management. *J Neurol Neurosurg Psychiatry* **81**, 358–67 (2010).
8. Miller, J. W. *et al.* Recruitment of human muscleblind proteins to (CUG)(n) expansions associated with myotonic dystrophy. *EMBO J* **19**, 4439–48 (2000).
9. Lin, X. *et al.* Failure of MBNL1-dependent post-natal splicing transitions in myotonic dystrophy. *Hum Mol Genet* **15**, 2087–97 (2006).
10. Kuyumcu-Martinez, N. M., Wang, G. S. & Cooper, T. A. Increased steady-state levels of CUGBP1 in myotonic dystrophy 1 are due to PKC-mediated hyperphosphorylation. *Mol Cell* **28**, 68–78 (2007).
11. Iwahashi, C. K. *et al.* Protein composition of the intranuclear inclusions of FXTAS. *Brain* **129**, 256–71 (2006).
12. Kalsotra, A. *et al.* A postnatal switch of CELF and MBNL proteins reprograms alternative splicing in the developing heart. *Proc Natl Acad Sci U S A* **105**, 20333–8 (2008).
13. Bland, C. S. *et al.* Global regulation of alternative splicing during myogenic differentiation. *Nucleic Acids Res* (2010).
14. Philips, A. V., Timchenko, L. T. & Cooper, T. A. Disruption of splicing regulated by a CUG-binding protein in myotonic dystrophy. *Science* **280**, 737–41 (1998).
15. Ho, T. H., Bundman, D., Armstrong, D. L. & Cooper, T. A. Transgenic mice expressing CUG-BP1 reproduce splicing mis-regulation observed in myotonic dystrophy. *Hum Mol Genet* **14**, 1539–47 (2005).
16. Savkur, R. S., Philips, A. V. & Cooper, T. A. Aberrant regulation of insulin receptor alternative splicing is associated with insulin resistance in myotonic dystrophy. *Nat Genet* **29**, 40–7 (2001).
17. Charlet, B. N. *et al.* Loss of the muscle-specific chloride channel in type 1 myotonic dystrophy due to misregulated alternative splicing. *Mol Cell* **10**, 45–53 (2002).
18. Begemann, G. *et al.* muscleblind, a gene required for photoreceptor differentiation in Drosophila, encodes novel nuclear Cys3His-type zinc-finger-containing proteins. *Development* **124**, 4321–31 (1997).
19. Teplova, M. & Patel, D. J. Structural insights into RNA recognition by the alternative-splicing regulator muscleblind-like MBNL1. *Nat Struct Mol Biol* **15**, 1343–51 (2008).
20. Ho, T. H. *et al.* Muscleblind proteins regulate alternative splicing. *EMBO J* **23**, 3103–12 (2004).
21. Cass, D. *et al.* The four Zn fingers of MBNL1 provide a flexible platform for recognition of its RNA binding elements. *BMC Mol Biol* **12**, 20 (2011).
22. Kanadia, R. N. *et al.* A muscleblind knockout model for myotonic dystrophy. *Science* **302**, 1978–80 (2003).
23. Fugier, C. *et al.* Misregulated alternative splicing of BIN1 is associated with T tubule alterations and muscle weakness in myotonic dystrophy. *Nature Medicine* **17**, 720–5 (2011).
24. Moraes, K. C., Wilusz, C. J. & Wilusz, J. CUG-BP binds to RNA substrates and recruits PARN deadenylase. *Rna* **12**, 1084–91 (2006).
25. Vlasova, I. A. *et al.* Conserved GU-rich elements mediate mRNA decay by binding to CUG-binding protein 1. *Mol Cell* **29**, 263–70 (2008).
26. Lee, J. E., Lee, J. Y., Wilusz, J., Tian, B. & Wilusz, C. J. Systematic analysis of cis-elements in unstable mRNAs demonstrates that CUGBP1 is a key regulator of mRNA decay in muscle cells. *PLoS One* **5**, e11201 (2010).
27. Rattenbacher, B. *et al.* Analysis of CUGBP1 Targets Identifies GU-Repeat Sequences That Mediate Rapid mRNA Decay. *Mol Cell Biol* **30**, 3970–80 (2010).
28. Timchenko, N. A., Iakova, P., Cai, Z. J., Smith, J. R. & Timchenko, L. T. Molecular basis for impaired muscle differentiation in myotonic dystrophy. *Mol Cell Biol* **21**, 6927–38 (2001).
29. Timchenko, N. A. *et al.* Overexpression of CUG triplet repeat-binding protein, CUGBP1, in mice inhibits myogenesis. *J Biol Chem* **279**, 13129–39 (2004).
30. Licatalosi, D. D. *et al.* HITS-CLIP yields genome-wide insights into brain alternative RNA processing. *Nature* **456**, 464–9 (2008).
31. Bailey, T. L. & Elkan, C. The value of prior knowledge in discovering motifs with MEME. *Proc Int Conf Intell Syst Mol Biol* **3**, 21–9 (1995).
32. Marquis, J. *et al.* CUG-BP1/CELF1 requires UGU-rich sequences for high-affinity binding. *Biochem J* **400**, 291–301 (2006).
33. Du, H. *et al.* Aberrant alternative splicing and extracellular matrix gene expression in mouse models of myotonic dystrophy. *Nat Struct Mol Biol* **17**, 187–93 (2010).
34. Goers, E. S., Purcell, J., Voelker, R. B., Gates, D. P. & Berglund, J. A. MBNL1 binds GC motifs embedded in pyrimidines to regulate alternative splicing. *Nucleic Acids Res* (2010).
35. Kino, Y. *et al.* Muscleblind protein, MBNL1/EXP, binds specifically to CHHG repeats. *Hum Mol Genet* **13**, 495–507 (2004).
36. Xue, Y. *et al.* Genome-wide analysis of PTB-RNA interactions reveals a strategy used by the general splicing repressor to modulate exon inclusion or skipping. *Mol Cell* **36**, 996–1006 (2009).
37. Hamada, H., Meno, C., Watanabe, D. & Saijoh, Y. Establishment of vertebrate left-right asymmetry. *Nat Rev Genet* **3**, 103–13 (2002).
38. Yashiro, K., Shiratori, H. & Hamada, H. Haemodynamics determined by a genetic programme govern asymmetric development of the aortic arch. *Nature* **450**, 285–8 (2007).
39. Dong, F. *et al.* Pitx2 promotes development of splanchnic mesoderm-derived branchiomeric muscle. *Development* **133**, 4891–9 (2006).
40. Shih, H. P., Gross, M. K. & Kioussi, C. Cranial muscle defects of Pitx2 mutants result from specification defects in the first branchial arch. *Proceedings of the National Academy of Sciences of the United States of America* **104**, 5907–12 (2007).
41. Gherzi, R. *et al.* Akt2-mediated phosphorylation of Pitx2 controls Ccnd1 mRNA decay during muscle cell differentiation. *Cell Death and Differentiation* **17**, 975–83 (2010).
42. Chen, H. H., Xu, J., Safarpour, F. & Stewart, A. F. LMO4 mRNA stability is regulated by extracellular ATP in F11 cells. *Biochem Biophys Res Commun* **357**, 56–61 (2007).
43. Zhang, L., Lee, J. E., Wilusz, J. & Wilusz, C. J. The RNA-binding protein CUGBP1 regulates stability of tumor necrosis factor mRNA in muscle cells: implications for myotonic dystrophy. *J Biol Chem* **283**, 22457–63 (2008).
44. Horb, L. D. & Horb, M. E. BrunoL1 regulates endoderm proliferation through translational enhancement of cyclin A2 mRNA. *Dev Biol* (2010).
45. Yeo, G. W. *et al.* An RNA code for the FOX2 splicing regulator revealed by mapping RNA-protein interactions in stem cells. *Nat Struct Mol Biol* **16**, 130–7 (2009).
46. Llorian, M. *et al.* Position-dependent alternative splicing activity revealed by global profiling of alternative splicing events regulated by PTB. *Nat Struct Mol Biol* **17**, 1114–23 (2010).
47. Hino, S. *et al.* Molecular mechanisms responsible for aberrant splicing of SERCA1 in myotonic dystrophy type 1. *Hum Mol Genet* **16**, 2834–43 (2007).
48. Sen, S. *et al.* Muscleblind-like 1 (Mbnl1) promotes insulin receptor exon 11 inclusion via binding to a downstream evolutionarily conserved intronic enhancer. *J Biol Chem* **285**, 25426–37 (2010).
49. Ule, J., Jensen, K., Mele, A. & Darnell, R. B. CLIP: a method for identifying protein-RNA interaction sites in living cells. *Methods* **37**, 376–86 (2005).
50. Li, H. & Durbin, R. Fast and accurate long-read alignment with Burrows-Wheeler transform. *Bioinformatics* **26**, 589–95 (2010).
51. Rhead, B. *et al.* The UCSC Genome Browser database: update 2010. *Nucleic Acids Res* **38**, D613–9 (2010).
52. Quinlan, A. R. & Hall, I. M. BEDTools: a flexible suite of utilities for comparing genomic features. *Bioinformatics* **26**, 841–2 (2010).
53. Huang da, W., Sherman, B. T. & Lempicki, R. A. Systematic and integrative analysis of large gene lists using DAVID bioinformatics resources. *Nat Protoc* **4**, 44–57 (2009).
54. Dennis, G., Jr. *et al.* DAVID: Database for Annotation, Visualization, and Integrated Discovery. *Genome Biol* **4**, P3 (2003).

Acknowledgements

This work was supported by a JST-DASTI joint grant entitled "Strategic Japanese-Danish Cooperative Program on Molecular Medical Research", by Grants-in-Aid from the MEXT and MHLW of Japan, and by a grant from the Danish Medical Research Council (FSS Grant no. 271-07-342).

Author contributions

A.M., H.S.A, T.O., and M.I. performed the experiments. A.M., T.K.D., B.S.A., and K.O. analyzed the data. A.M., T.K.D., B.S.A. and K.O. prepared the manuscript. All authors reviewed the manuscript.

Additional information

Accession codes: All HITS-CLIP data were registered in ArrayExpress with an accession number E-MTAB-414 and in ENA with an accession number ERP000789.

All microarray data were uploaded to the Gene Expression Omnibus database with accession numbers, GSE29990 for exon arrays and GSE27583 for expression arrays.

Supplementary information accompanies this paper at http://www.nature.com/scientificreports

Competing financial interests: The authors declare no competing financial interests.

How to cite this article: Masuda, A. *et al.* CUGBP1 and MBNL1 preferentially bind to 3′ UTRs and facilitate mRNA decay. *Sci. Rep.* **2**, 209; DOI:10.1038/srep00209 (2012).

Myasthenic syndrome caused by plectinopathy

D. Selcen, MD
V.C. Juel, MD
L.D. Hobson-Webb, MD
E.C. Smith, MD
D.E. Stickler, MD
A.V. Bite, BS
K. Ohno, MD, PhD
A.G. Engel, MD

Address correspondence and reprint requests to Dr. Andrew G. Engel, Department of Neurology, Mayo Clinic, Rochester, MN 55905
age@mayo.edu

ABSTRACT

Background: Plectin crosslinks intermediate filaments to their targets in different tissues. Defects in plectin cause epidermolysis bullosa simplex (EBS), muscular dystrophy (MD), and sometimes pyloric atresia. Association of EBS with a myasthenic syndrome (MyS) was documented in a single patient in 1999.

Objectives: To analyze the clinical, structural, and genetic aspects of a second and fatal case of EBS associated with a MyS and search for the genetic basis of the disease in a previously reported patient with EBS-MD-MyS.

Methods: Clinical observations; histochemical, immunocytochemical, and electron microscopy studies of skeletal muscle and neuromuscular junction; and mutation analysis.

Results: An African American man had EBS since early infancy, and progressive muscle weakness, hyperCKemia, and myasthenic symptoms refractory to therapy since age 3 years. Eventually he became motionless and died at age 42 years. At age 15 years, he had a marked EMG decrement, and a reduced miniature endplate potential amplitude. The myopathy was associated with dislocated muscle fiber organelles, structurally abnormal nuclei, focal plasmalemmal defects, and focal calcium ingress into muscle fibers. The neuromuscular junctions showed destruction of the junctional folds, and remodeling. Mutation analysis demonstrated a known p.Arg2319X and a novel c.12043dupG mutation in *PLEC1*. The EBS-MD-MyS patient reported in 1999 also carried c.12043dupG and a novel p.Gln2057X mutation. The novel mutations were absent in 200 Caucasian and 100 African American subjects.

Conclusions: The MyS in plectinopathy is attributed to destruction of the junctional folds and the myopathy to defective anchoring of muscle fiber organelles and defects in sarcolemmal integrity. ***Neurology*® 2011;76:327–336**

GLOSSARY

Ab = antibodies; **AChR** = acetylcholine receptor; **anti-C Ab** = antibody recognizing the C-terminal plectin domain; **anti-Rod Ab** = antibody recognizing the plectin rod domain; **EBS** = epidermolysis bullosa simplex; **EP** = endplate; **IF** = intermediate filament; **IgG** = immunoglobulin G; **MD** = muscular dystrophy; **MyS** = myasthenic syndrome; **P1** = patient 1; **P2** = patient 2.

Plectin is a ~500 kDa dumbbell-shaped molecule with a central coiled-coil rod domain flanked by globular N- and C-terminal domains. Owing to tissue and organelle-specific transcript isoforms, plectin is a versatile linker of cytoskeletal components to target organelles in cells of different tissues.[1–3] In skeletal muscle, multiple alternatively spliced transcripts of exon preceding common exon 2 link desmin intermediate filaments (IFs) to specific targets: the outer nuclear membrane (isoform 1), the outer mitochondrial membrane (isoform 1b), Z disks (isoform 1 d), and costameres in the sarcolemma (isoform 1f).[3] Plectin is also highly expressed at the neuromuscular junction where it provides crucial structural support for the junctional folds.[4] Plectin deficiency in muscle results in progressive muscular dystrophy (MD).[4–19] Plectin

Supplemental data at www.neurology.org

From the Department of Neurology (D.S., A.V.B., K.O., A.G.E.), Mayo Clinic, Rochester, MN; the Department of Neurology (V.C.J., L.D.H.-W., E.C.S.), Duke University School of Medicine, Durham, NC; and the Department of Neurosciences (D.E.S.), Medical University of South Carolina, Charleston. K.O. is currently affiliated with the Center for Neurological Diseases and Cancer, Nagoya University, Japan.

Study funding: Supported by a grant from the National Institute of Neurological Disorders and Stroke RO1-NS 6277 (A.G.E.) and a research grant from the Muscular Dystrophy Association (A.G.E.).

Disclosure: Author disclosures are provided at the end of the article.

is also highly expressed in intercalated disks in the heart but only a single patient with EBS/MD and cardiomyopathy was identified to date.[18] Plectin deficiency in skin causes epidermolysis bullosa simplex (EBS).[20] Some patients with EBS and MD (EBS-MD) also had symptoms suggesting a myasthenic disorder[9,21–23] but this was not suspected or confirmed by specific studies. The association of EBS-MD with a myasthenic syndrome (MyS) was well-documented in a single patient (P1) in 1999.[4] Although numerous autosomal recessive and one dominant mutation in *PLEC* have been detected,[20] the genetic basis of EBS-MD-MyS in P1 was not identified. We describe our findings in a second patient with EBS-MD-MyS (P2), report additional observations in P1, and identify the genetic basis of the disease in both patients.

METHODS All human studies described here were in accord with the guidelines of the Institutional Review Board of the Mayo Clinic.

Structural observations. Routine histochemical studies on cryostat sections and electron microscopy studies were performed as previously described.[24] Immunoglobulin G and the C3 and C9 complement components were immunolocalized as previously reported.[25,26] We immunolocalized the last 50 C-terminal residues of plectin with 4 μg/mL goat polyclonal C-20 antibody (anti-C Ab), and the plectin rod domain with 4 μg/mL 10F6 mouse monoclonal antibody (anti-Rod Ab) (both from Santa Cruz Biotechnology), followed by 3 μg/mL biotinylated donkey antigoat or antimouse immunoglobulin G (IgG) (Jackson ImmunoResearch Laboratories) and the ABC peroxidase kit (Vector Laboratories). Intrafiber calcium excess was evaluated by the Alizarin red stain.[27] Synaptic contact regions were visualized on fixed, teased muscle fibers by a cytochemical reaction for acetylcholinesterase.[28] The acetylcholine receptor (AChR) and plectin were colocalized at endplates (EPs) with rhodamine-labeled α-bungarotoxin and the plectin anti-Rod Ab followed by fluorescent goat antimouse IgG. EPs were localized for electron microscopy[24] and quantitatively analyzed[29] by established methods. Peroxidase-labeled α-bungarotoxin was used for the ultrastructural localization of AChR.[30]

Molecular genetic studies. Genomic DNA was isolated from blood of P1 and muscle of P2 and mRNA from intercostal muscles of both by standard methods. *PLEC* nucleotides were numbered according to the mRNA sequence (GenBank reference no: NM_000445). We used PCR primer pairs to amplify and directly sequence the 32 exons and flanking noncoding regions of *PLEC* isoform 1 and also first exons of isoforms 1b, 1d, and 1f. We screened for the identified novel mutations in 200 Caucasian and 100 African American control subjects using allele-specific PCR. To estimate expression of the rodless isoform of *PLEC* at the mRNA level, we used real-time PCR and SYBR green I (Roche) with 5′ GTGTCATCCAGGAGTACGTG 3′ as the forward primer in exon 30, 5′ AGCGACAGCAGAGTGACCAT 3′ as the forward primer in exon 31 that encodes the rod domain, 5′ GCCTTCTCCTGCTCGATGAA 3′ as the reverse primer in exon 32 for both forward primers, and *GAPDH* as the housekeeping gene. All experiments were done in triplicate.

RESULTS **Clinical observations.** P1 is an African American woman. Her case was reported in 1999 when she was 23 years of age.[4] In brief, she was diagnosed with EBS as an infant and her myasthenic symptoms began around the age of 9 years. Since 1999, her weakness has worsened so she can now only take a few steps, has dysphagia, is dyspneic on slight exertion and at night, and is resistant to anticholinesterase drugs. However, her skin symptoms are mild, with new skin blisters appearing infrequently.

P2 is an African American man. He was a single child without similarly affected family members. He sucked poorly during infancy but this gradually improved. Since the age of 6 weeks, he had an intermittent vesicular eruption over his skin and oral mucosa and developed nail deformities. He attained his motor milestones on time, but had significant fatigue on exertion since age 3 years. At age 11 years he had difficulty running and rising from the floor and serum creatine kinase level was 827 U/L (normal <60 U/L). Prednisone therapy improved his strength but was discontinued because of abdominal pain. Nystatin therapy for thrush worsened the weakness. At age 12 years, a vastus medialis muscle specimen revealed a myopathy associated with necrotic and regenerating fibers, a sural nerve specimen was normal, and a skin biopsy showed EBS and secondary infection. In 1981, at age 15 years, the patient was evaluated at the Mayo Clinic. He now had reduced muscle bulk, bilateral eyelid ptosis, restricted eye movements, and mild facial and moderately severe diffuse cervical and limb muscle weakness, and was areflexic except at the ankles. Nerve conduction studies were normal. Repetitive stimulation at 2 Hz showed a decremental response (67% in hypothenar muscles) that was partially corrected by IV edrophonium chloride. Serratus anterior and intercostal muscles were biopsied. In vitro electrophysiology study of the intercostal specimen by Dr. Edward Lambert revealed reduction of the mean miniature endplate potential amplitude to 50% of normal; the quantal content of the endplate potential was in the low-normal range. Tests for anti-AChR antibodies were negative. A MyS was diagnosed but therapy with pyridostigmine bromide for a year was of no benefit. The weakness progressed more rapidly throughout adolescence and accelerated after routine illnesses. At age

Figure 1 Patient photographs

(A, B) Patient at age 17 years. Note severe asymmetric bilateral ptosis, hyperactive frontalis muscle, facial paresis, open mouth, cubitus valgus, Achilles tendon contractures, and diffuse muscle atrophy. (C, D) Patent at age 41 years. He has a tracheostomy, has facial diplegia, is unable to close his mouth or open his eyes, and shows the chronic skin changes of epidermolysis bullosa simplex. He also has blisters on his lip and tongue and oral moniliasis.

17 years, he could barely walk (figure 1, A and B). He was wheelchair-bound by age 18 years, and respirator-dependent by age 26 years. After age 35 years, he had dysarthria and dysphagia and needed a percutaneous gastrostomy. His cognitive functions and cardiac status remained normal. Subsequently, he became motionless (figure 1C), continued to have skin blisters (figure 1D), communicated with clicks and whispers, failed to respond to 3,4-diaminopyridine combined with pyridostigmine bromide, and died of pneumonia at age 42 years.

Histochemistry, P2. Serratus anterior and intercostal muscle specimens showed similar findings (figure 2, A and B). The muscle fiber diameters varied from 6 μm to ~120 μm. There was a mild to moderate increase of internal nuclei. Many nuclei were larger than normal and appeared in subsarcolemmal rows or clusters. Some fibers were necrotic or regenerating or subdividing by splitting, or displayed aberrant myofibrils. There was mild to marked (figure 2B) increase of perimysial and endomysial connective tissue. No immunoglobulin G, C3, or C9 deposits were present at patient endplates. In sections reacted for oxidative enzymes, some fibers showed attenuation or an irregular distribution of enzyme activity. Both muscle specimens showed type 1 fiber preponderance. Because plectin deficiency disconnects or weakens the link between the sarcolemma and the underlying cytoskeleton, it likely increases sarcolemmal vulnerability to mechanical stress. We therefore searched for signs of sarcolemmal injury evidenced by subsarcolemmal calcium deposits[27] and detected these in scattered fibers in both patients (figure 2C and figure e-1 [on the *Neurology*® Web site at www.neurology.org]).

Plectin immunostains. These were performed on 6- to 10-μm-thick acetone fixed frozen sections. In 1999, an antibody recognizing the rod domain of plectin (gift from Dr. Owaribe) showed no immunoreactivity in P1 muscle fibers. As this antibody was no longer available, we used the 10F6 antibody directed against the plectin rod domain (anti-Rod Ab), and a C-20 antibody raised against the last 50 C-terminal residues of plectin (anti-C Ab), and immunolocalized plectin in P1, P2, and normal muscle (see Methods). In normal muscle, both antibodies immunostained the sarcolemma, the intermyofibrillar network, capillaries, and vascular smooth muscle (figure 2, E and H); the C-20 Ab also immunostained perineurium and myelin-

Figure 2 **Histochemistry and plectin localization studies in patient 2**

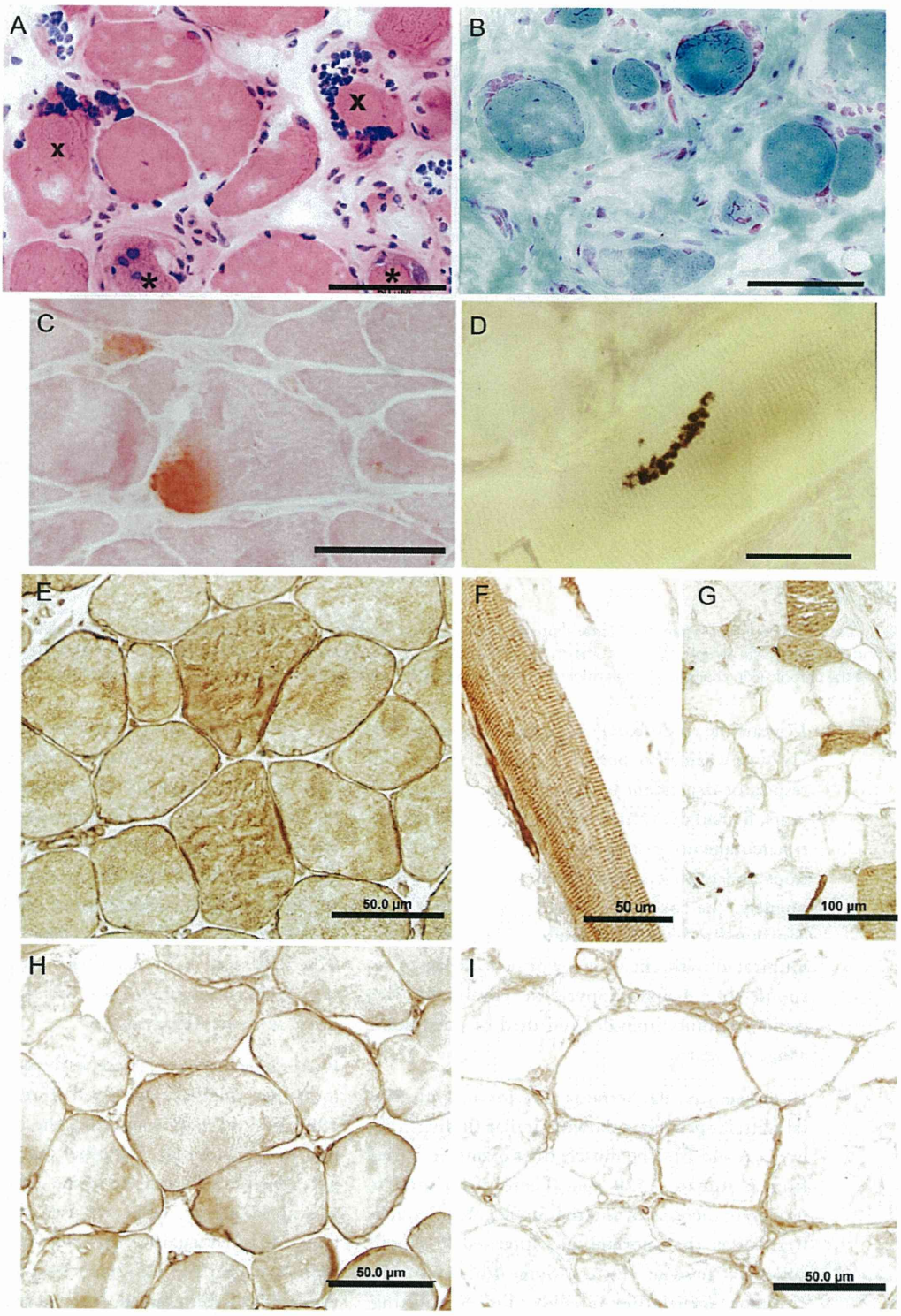

(A, B) Note marked variation in fiber size, regenerating fiber elements (asterisks), endomysial fibrosis (B), and clusters of large nuclei at periphery of several fibers. (C) Alizarin red stain reveals focal calcium deposits in 2 fibers. (D) Multiple small cholinesterase-reactive endplate regions arrayed over an extended length of the fiber. Plectin was localized in normal control muscle (E, H) and patient intercostal muscle (F, G, I) with antibody recognizing the plectin rod domain (anti-Rod Ab) (E–G) and antibody recognizing the C-terminal plectin domain (anti-C Ab) (H, I). (E, H) In normal muscle, plectin is localized to the sarcolemma and sarcoplasm with both Abs. The anti-Rod Ab shows plectin-depleted and plectin-positive muscle fibers (F, G), whereas the anti-C Ab shows sarcoplasmic loss and slight sarcolemmal expression of plectin in all muscle fibers (I). Bars indicate 50 μm in all panels except in (G), where they indicate 100 μm.

Figure 3 **Ultrastructural findings in abnormal muscle fibers of patient 2**

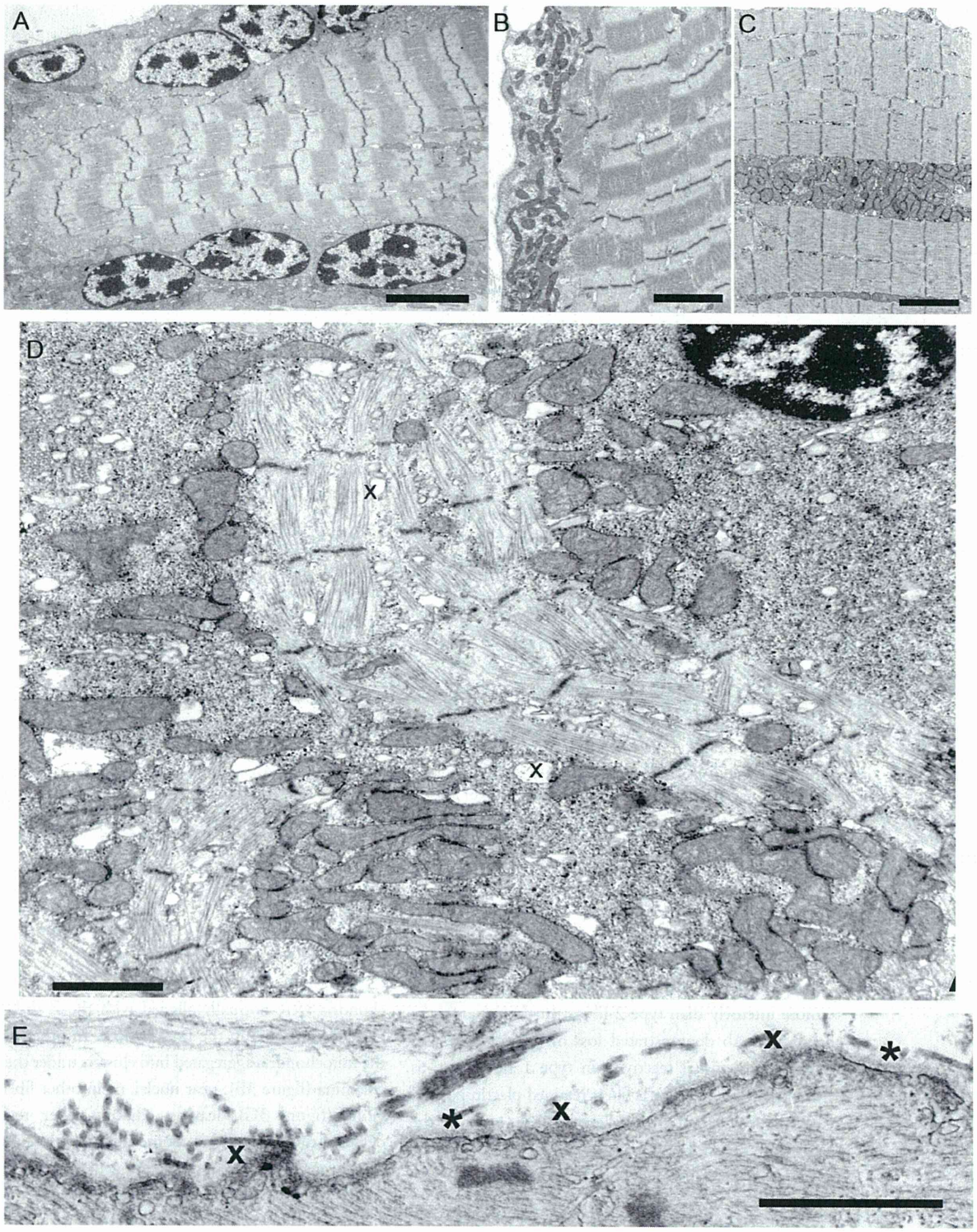

(A) Note subsarcolemmal rows of large nuclei harboring multiple prominent chromatin bodies. (B, C) Subsarcolemmal and intrafiber clusters of mitochondria surrounded by fiber regions devoid of mitochondria. (D) Aberrant and disrupted myofibrils surrounded by clusters of mitochondria intermingled with glycogen, ribosomes, and dilated vesicles (x). Note preapoptotic nucleus at upper right. (E) Focal sarcolemma defects due to gaps in the plasma membrane. Where the plasma membrane is absent, the overlying basal lamina is thickened (x). Small vesicles underlie the thickened basal lamina. Asterisks indicate segments of the preserved plasma membrane. Bars = 4 μm in (A), 3 μm (B, C), 1.4 μm in (D), 1 μm in (E).

Figure 4 **Abnormal endplate (EP) regions in patient 2**

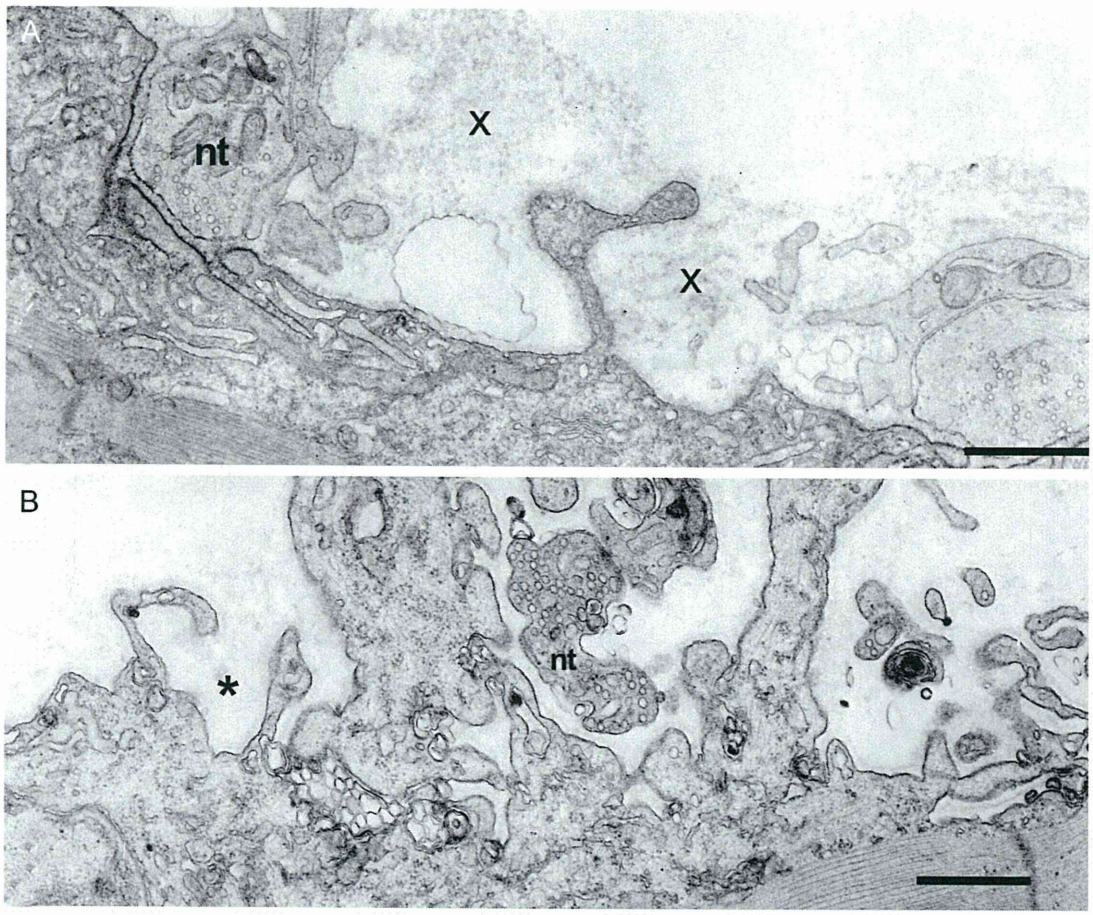

(A) The imaged EP regions show partial occupancy of the postsynaptic region by the nerve terminal and remnants of degenerate folds (x). The nerve terminal (nt) occupies only part of the postsynaptic region. Degenerate remnants of the folds (x) appear over the simplified postsynaptic region from which folds were lost. Dark reaction product on postsynaptic membrane shows acetylcholine receptor localization with peroxidase labeled α-bungarotoxin. (B) Small nerve terminal occupies only part of a highly simplified postsynaptic region. Asterisk indicates remnants of basal lamina that surrounded preexisting folds. Bars = 1 μm.

ated nerve fibers (not shown). In normal muscle, the anti-Rod Ab (figure 2E) was more reactive than the anti-C antibody (figure 2H) and stained type 1 fibers more intensely than type 2 fibers. In the patients, the anti-Rod Ab demonstrated loss of sarcoplasmic and trace sarcolemmal reactivity in type 1 fibers but, as noted by others,[19] type 2 fibers retained plectin positivity (figure 2, F and G, and figure e-2). In contrast, the C-20 Ab revealed no sarcoplasmic and only slight sarcolemmal reactivity in all fibers (figure 2I).

Muscle fiber ultrastructure in P2. ***Nuclear abnormalities.*** Consistent with light microscopy, numerous muscle fibers harbored subsarcolemmal rows or clusters of large ovoid nuclei containing 3 to 10 large, highly electron dense chromatin deposits (figure 3A). Nuclei in other fiber regions were of normal size and heterochromatic or euchromatic. Some nuclei harbored large clumps of heterochromatin with small islands of euchromatin indicating preapoptotic changes (figure 3D).

Mitochondrial abnormalities. In some fibers, the mitochondria were normally aligned with the Z disk and evenly distributed in the muscle fiber. In other fibers, the mitochondria aggregated into clusters under the sarcolemma (figure 3B), near nuclei, or in other fiber regions (figure 3C), leaving adjacent fiber regions depleted of mitochondria. Some mitochondrial aggregates were interspersed with glycogen granules, ribosomes, and dilated vesicles (figure 3D).

Myofibrillar abnormalities. Aberrant myofibrils appeared among dislocated organelles in both atrophic and nonatrophic fibers (figure 3D). Disintegration and streaming of Z disks were detected in some fiber regions with or without myofibrillar disarray. A few abnormal fiber regions harbored small nemaline rods. End-stage muscle fibers contained few mitochondria, remnants of

Figure 5 Plectin domains and identified *PLEC* variants

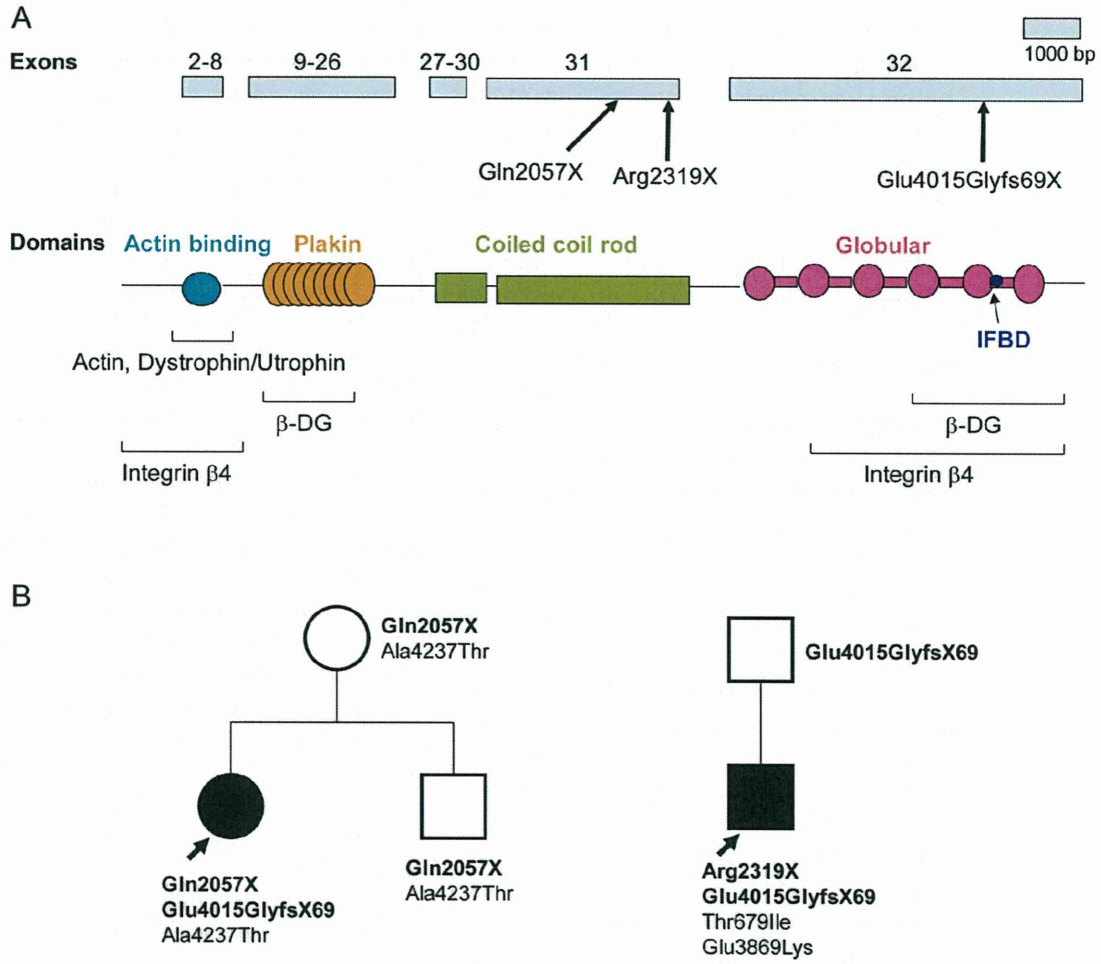

(A) Schematic representation of *PLEC* exons 2–32 indicating identified patient mutations and binding domains associated with C- and N-terminal regions of plectin.[39] (B) Family analysis of P1 and P2 shows transmission of pathogenic mutations (bold face) and polymorphisms.

Z disks with attached short filaments (Z brushes), and debris. Small membrane-bound vacuoles of different sizes that likely represent dilated components of the sarcoplasmic reticulum appeared in fiber regions with or without other abnormalities (figure 3D).

Sarcolemmal defects. The focal subsarcolemmal calcium deposits in scattered muscle fibers prompted us to search for sarcolemmal defects at the ultrastructural level and we detected these in some fibers of both patients. Where the plasma membrane was discontinuous, it was often covered by focally thickened basal lamina (figure 3E).

Endplate studies in P2. Synaptic contacts on the muscle fibers, visualized by the cholinesterase reaction, consisted of multiple small EP regions arrayed over an extended length of the muscle fiber (figure 2D). This finding has been observed in other patients with ongoing destruction and remodeling of the postsynaptic region.[31]

Colocalization of plectin and AChR by fluorescence microscopy showed strong expressions of plectin and AChR at normal EPs. At patient EPs AChR expression was not appreciably attenuated but plectin expression was barely perceptible (figure e-3).

On electron microscopy, some EP regions appeared normal but many had an abnormal conformation, displaying one or more of the following: partial occupancy of the postsynaptic region by nerve terminals, small nerve terminals, atrophic and remnants of degenerated junctional folds resulting in highly simplified postsynaptic regions, and nerve sprouts near degenerating EPs (figure 4 and figure e-4). Table e-1 shows the frequency of the observed conformational changes. Table e-2 shows morphometry revealing reduced size of presynaptic and postsynaptic EP components.

Genetic analysis. Genetic analysis was challenging owing to the very large size of the *PLEC* transcript

(~14 Kb vs ~11 Kb for dystrophin), the very large exons 31 (3381 bp) and 32 (6219 bp), multiple splice variants of exon 1, and polymorphisms that may be race-dependent. Eventually we detected 2 truncating mutations in each patient (figure 5). P1 harbors a stop codon mutation at nucleotide 6169 in exon 31 (c.6169C>T/p.Gln2057X), and a duplication at nucleotide 12043 in exon 32 that predicts 68 missense codons followed by a stop codon (c.12043dupG/p.Glu4015GlyfsX69). P2 harbors a previously reported nonsense mutation at nucleotide 6955 in exon 31 which generates a stop codon (c.6955C>T/p.Arg2319X),[16] and the same duplication mutation detected in P1 (figure 5B). Presence of the pathogenic mutation was confirmed at the cDNA level in both patients. Both stop codon mutations abrogate, and the c.12043dupG mutation disrupts, the IF binding site and one of the two β-dystroglycan and integrin β4 binding sites (figure 5A).

Both patients also harbored polymorphisms not listed in the SNP database (see figure 5B). In P1, p.Ala4237Thr was deemed a polymorphism because it appeared together with Gln2057X in the unaffected mother. In P2, p.Thr679Ile was present in 1 of 60 African Americans and p.Glu3869Lys in 1 of 100 African Americans, although both variants were absent in 200 Caucasians.

It has been suggested that expression of the rodless plectin transcript may mitigate the plectinopathy phenotype.[32] We therefore confirmed presence of the rodless domain by sequencing cDNA and used real-time PCR to compare the relative abundance of the rodless transcript in P1, P2, and 3 normal controls. The rodless transcript/full transcript ratio was 0.15 in P1, 0.32 in P2, and 0.22 ± 0.03 (mean ± SD) in 3 controls.

DISCUSSION Although each patient carries a nonsense mutation in *PLEC* exon 31 and an identical frameshift mutation in exon 32, the tempo of the disease was faster in P2 than in P1. In P2, EBS presented at age 6 weeks, MyS at age 3 years, and he lost ambulation by age 18 years. In P1, MyS presented at age 9 years, EBS at age 18 years, and she can still take a few steps at age 31 years. It has been suggested that expression of the rodless transcript can mitigate the phenotype in patients who carry mutations in the plectin rod domain.[32] However, real-time PCR indicates that expression of the rodless transcript was higher in the more severely affected P2. Thus in the patients studied by us the abundance of the rodless transcript was not a reliable indicator of the clinical phenotype.

Dislocation of the fiber organelles apparent at the ultrastructural level has multiple predictable consequences. Abnormal alignment and displacement of the myofibrils weakens or eliminates their contractile strength; separation of mitochondria from myofibrils renders energy delivery to contracting myofibrils inefficient. The eccentrically positioned large nuclei with multiple chromatin deposits may be dysfunctional or inefficient in their translational activities and in nuclear-cytoplasmic trafficking when not adjacent to organelles or fiber domains they subserve. Injury to the inadequately supported plasma membrane is evidenced by subsarcolemmal calcium deposits and sarcolemmal defects in a proportion of the fibers (see figure 2C, figure 3E, and figure e-1). Most of these were smaller than those in Duchenne dystrophy[27,33] but they still likely contribute to fiber injury and, if large, they may contribute to fiber necrosis.

Electron microscopy of the EPs indicates that plectin deficiency targets the junctional folds for destruction. When sarcomeres contract and relax, the extrajunctional sarcolemma bulges and relaxes but the junctional folds maintain a constant architecture.[34] This mandates enhanced rigidity of the junctional folds and renders them especially vulnerable to mechanical stress. Thus loss of cytoskeletal support of the junctional folds due to the plectin deficiency, as depicted in figure e-3, readily explains the progressive destruction of the folds. Destruction of junctional folds decreases the density or eliminates the voltage-gated Na^+ channels which are concentrated in troughs between the folds[35,36] and this increases the threshold for action potential generation.[37] Destruction of the folds also decreases the input resistance of the postsynaptic membrane and thereby the amplitude of synaptic potential.[38] Widening of the synaptic space reduces the concentration of acetylcholine before it reaches the junctional folds. The combination of these factors decreases quantal efficacy and compromises the safety margin of neuromuscular transmission. The relentless progression of the myasthenic symptoms in both patients implies that formation of new EP regions eventually fails to compensate for the ongoing destructive changes.

Why only a proportion of the muscle fibers is affected in a given muscle, and why some EPs are more severely affected than others, remain unanswered questions. It is uncertain that it can be attributed to preserved plectin expression in type 2 fibers, as shown by the 10F6 anti-Rod antibody. First, the anti-C terminal antibody showed nearly complete plectin deficiency in all muscle fibers in both patients. Second, the anti-rod domain antibody showed either no plectin reactivity in any fiber, or preserved immunoreactivity in type 1 instead of type 2 fibers.[19]

The fiber type specificities of the different anti-rod domain antibodies in plectinopathy are presently unexplained.

It is also unclear why some patients with EBS-MD have myasthenic symptoms and others do not. Possibly myasthenic weakness of the limb muscles is masked by the MD, or is overlooked in severely weak patients, but fatigable weakness of the oculobulbar muscles would be unlikely to go unrecognized. It also is not known whether some mutations are more prone to result in the MyS phenotype than others.

ACKNOWLEDGMENT

The authors thank Drs. Neill Graff-Radford and Nilufer Ertekin-Taner for anonymated DNA samples from African American control subjects.

DISCLOSURE

Dr. Selcen reports no disclosures. Dr. Juel has received research support from Alexion Pharmaceuticals, Inc. Dr. Hobson-Webb has served as a consultant for Novella Clinical Inc. and has received research support from Genzyme Corporation and AANEM Foundation. Dr. Smith reports no disclosures. Dr. Stickler has received research support from Agency for Toxic Substances and Disease Registry, Centers for Disease Control and Prevention (CDC) and has served as an expert witness in a legal proceeding. Ms. Bite reports no disclosures. Dr. Ohno has received Grants-in-Aid from the Japan Society for the Promotion of Science, the Ministry of Health, Labour and Welfare, and the Japan Science and Technology Agency. Dr. Engel serves as an Associate Editor of *Neurology*; receives publishing royalties for *Myology 3rd ed.* (McGraw-Hill, 2004); and has received research support from the NIH and the Muscular Dystrophy Association.

Received June 21, 2010. Accepted in final form September 21, 2010.

REFERENCES

1. Elliott CE, Becker B, Oehler S, Castanon MJ, Hauptmann R, Wiche G. Plectin transcript diversity: identification and tissue distribution of variants with distinct first coding exons and rodless isoforms. Genomics 1997;42:115–125.
2. Fuchs P, Zorer M, Rezniczek GA, et al. Unusual 5′ transcript complexity of plectin isoforms: novel tissue-specific exons modulate actin binding activity. Hum Mol Genet 1999;8:2461–2472.
3. Konieczny P, Fuchs P, Reipert S, et al. Myofiber integrity depends on desmin network targeting to Z-disks and costameres via distinct plectin isoforms. J Cell Biol 2008;181:667–681.
4. Banwell BL, Russel J, Fukudome T, Shen X-M, Stilling G, Engel AG. Myopathy, myasthenic syndrome, and epidermolysis bullosa simplex due to plectin deficiency. J Neuropathol Exp Neurol 1999;58:832–846.
5. McLean W, Pulkkinen L, Smith F, et al. Loss of plectin causes epidermolysis bullosa with muscular dystrophy: cDNA cloning and genomic organization. Genes Dev 1996;10:1724–1735.
6. Smith FJ, Eady R, Leigh I, et al. Plectin deficiency results in muscular dystrophy and epidermolysis bullosa simplex. Nat Genet 1996;13:450–457.
7. Chavanas S, Pulkkinen L, Gache Y, et al. A homozygous nonsense mutation in the *PLEC1* gene in patients with epidermolysis bullosa simplex with muscular dystrophy. J Clin Invest 1996;98:2196–2200.
8. Pulkkinen L, Smith F, Shimizu H, et al. Homozygous deletion mutations in the plectin gene (PLEC1) in patients with epidermolysis bullosa simplex associated with late-onset muscular dystrophy. Hum Mol Genet 1996;5:1539–1546.
9. Gache Y, Chavanas S, Lacour J, et al. Defective expression of plectin/HD1 in epidermolysis bullosa simplex with muscular dystrophy. J Clin Invest 1996;97:2289–2298.
10. Mellerio J, Smith F, McMillan J, et al. Recessive epidermolysis bullosa simplex associated with plectin mutations: infantile respiratory complications in two unrelated cases. Br J Dermatol 1997;137:898–906.
11. Dang M, Pulkkinen L, Smith F, McLean W, Uitto J. Novel compound heterozygous mutations in the plectin gene in epidermolysis bullosa with muscular dystrophy and the use of protein truncation test for detection of premature termination codon mutations. Lab Invest 1998;78:195–204.
12. Takizawa Y, Shimizu H, Rouan F, et al. Four novel plectin gene mutations in Japanese patients with epidermolysis bullosa and muscular dystrophy disclosed by heteroduplex scanning and protein truncation tests. J Invest Dermatol 1999;112:109–112.
13. Shimizu H, Takizawa Y, Pulkkinen L, et al. Epidermolysis bullosa simplex associated with muscular dystrophy: phenotype-genotype correlations and review of the literature. J Am Acad Dermatol 1999;41:950–956.
14. Rouan F, Pulkkinen L, Meneguzzi G, et al. Epidermolysis bullosa: novel and de novo premature termination codon and deletion mutations in the plectin gene predict late-onset muscular dystrophy. J Invest Dermatol 2000;114:381–387.
15. Bauer JW, Rouan F, Kofler B, et al. A compound heterozygous one amino-acid insertion/nonsense mutation in the plectin gene causes epidermolysis bullosa simplex with plectin deficiency. Am J Pathol 2001;158:617–625.
16. Takahashi Y, Rouan F, Uitto J, et al. Plectin deficient epidermolysis bullosa simplex with 27-year-history of muscular dystrophy. J Dermatol Sci 2005;37:87–93.
17. Pfendner E, Rouan F, Uitto J. Progress in epidermolysis bullosa: the phenotypic spectrum of plectin mutations. Exp Dermatol 2005;14:241–249.
18. Bolling MC, Pas HH, De Visser M, et al. PLEC1 mutations underlie adult-onset dilated cardiomyopathy in epidermolysis bullosa simplex with muscular dystrophy. J Invest Dermatol 2010;130:1178–1181.
19. McMillan JR, Akiyama M, Rouan F, et al. Plectin defects in epidermolysis bullosa simplex with muscular dystrophy. Muscle Nerve 2007;35:24–35.
20. Rezniczeck GA, Walko G, Wiche G. Plectin defects lead to various forms of epidermolysis bullosa simplex. Dermatol Clin 2009;28:33–41.
21. Niemi K, Sommer H, Kero M, Kanerva L, Haltia M. Epidermolysis bullosa simplex associated with muscular dystrophy with recessive inheritance. Arch Dermatol 1988;124:551–554.
22. Fine J-D, Stenn J, Johnson L, Wright T, Bock H, Horiguchi Y. Autosomal recessive epidermolysis bullosa simplex. Arch Dermatol 1989;125:931–938.
23. Doriguzzi C, Palmucci L, Mongini T, et al. Congenital muscular dystrophy associated with familial junctional epidermolysis bullosa letalis. Eur Neurol 1993;33:454–460.

24. Engel AG. The muscle biopsy. In: Engel AG, Franzini-Armstrong C, eds. Myology, 3rd ed. New York: McGraw-Hill; 2004:681–690.
25. Engel AG, Lambert EH, Howard FM. Immune complexes (IgG and C3) at the motor end-plate in myasthenia gravis: ultrastructural and light microscopic localization and electrophysiologic correlations. Mayo Clin Proc 1977;52:267–280.
26. Sahashi K, Engel AG, Lambert EH, Howard FM Jr. Ultrastructural localization of the terminal and lytic ninth complement component (C9) at the motor end-plate in myasthenia gravis. J Neuropathol Exp Neurol 1980;39:160–172.
27. Bodensteiner JB, Engel AG. Intracellular calcium accumulation in Duchenne dystrophy and other myopathies: a study of 567,000 muscle fibers in 114 biopsies. Neurology 1978;28:439–446.
28. Gautron J. Cytochimie ultrastructurale des acétylcholinestérases. Microscopie 1974;21:259–264.
29. Engel AG. Quantitative morphological studies of muscle. In: Engel AG, Franzini-Armstrong C, eds. Myology, 2nd ed. New York: McGraw-Hill; 1994:1018–1045.
30. Engel AG, Lindstrom JM, Lambert EH, Lennon VA. Ultrastructural localization of the acetylcholine receptor in myasthenia gravis and in its experimental autoimmune model. Neurology 1977;27:307–315.
31. Engel AG, Lambert EH, Mulder DM, et al. A newly recognized congenital myasthenic syndrome attributed to a prolonged open time of the acetylcholine-induced ion channel. Ann Neurol 1982;11:553–569.
32. Nastsuga K, Nishie W, Akiyama M, et al. Plectin expression patterns determine two distinct subtypes of epidermolysis bullosa simplex. Hum Mutat 2010;31:308–316.
33. Mokri B, Engel AG. Duchenne dystrophy: electron microscopic findings pointing to a basic or early abnormality in the plasma membrane of the muscle fiber. Neurology 1975;25:1111–1120.
34. Ruff RL. Effects of length changes on Na^+ current amplitude and excitability near and far from the end-plate. Muscle Nerve 1996;19:1084–1092.
35. Flucher BE, Daniels MP. Distribution of Na^+ channels and ankyrin in neuromuscular junctions is complementary to that of acetylcholine receptors and the 43 kd protein. Neuron 1989;3:163–175.
36. Ruff RL, Whittlesey D. Na^+ current density and voltage dependence in human intercostal muscle fibers. J Physiol 1992;458:85–97.
37. Ruff RL, Lennon VA. How myasthenia gravis alters the safety factor of neuromuscular transmission. J Neuroimmunol 2008;15:13–20.
38. Martin AR. Amplification of neuromuscular transmission by postjunctional folds. Proc R Soc Lond B 1994;258:321–326.
39. Konieczny P, Wiche G. Muscular integrity: a matter of interlinking distinct structures via plectin. In: Lang NG, ed. The Sarcomere and Skeletal Muscle Disease. New York: Springer; 2009:165–175.

Parkinsonism and Related Disorders 17 (2011) 46–49

Contents lists available at ScienceDirect

Parkinsonism and Related Disorders

journal homepage: www.elsevier.com/locate/parkreldis

Urinary 8-hydroxydeoxyguanosine correlate with hallucinations rather than motor symptoms in Parkinson's disease☆

Masaaki Hirayama [a,*], Tomohiko Nakamura [a], Hirohisa Watanabe [a], Kei Uchida [a], Tetsuo Hama [a], Takashi Hara [a], Yoshiki Niimi [a], Mizuki Ito [a], Kinji Ohno [b], Gen Sobue [a,*]

[a] Department of Neurology, Nagoya University Graduate School of Medicine, 65 Tsurumai-cho, Showa-ku, Nagoya 466-8550, Japan
[b] Division of Neurogenetics, Center for Neurological Diseases and Cancer, Nagoya University Graduate School of Medicine, 65 Tsurumai-cho, Showa-ku, Nagoya 466-8550, Japan

ARTICLE INFO

Article history:
Received 11 August 2010
Received in revised form
27 October 2010
Accepted 1 November 2010

Keywords:
Parkinson's disease
8-Hydroxydeoxyguanosine
Hallucination
Oxidative stress
Non-motor symptom

ABSTRACT

Background: Oxidative stress is causally associated with the pathogenesis of Parkinson's disease (PD). Oxygen generates a large amount of reactive oxygen species (ROS). ROS including hydroxyl radicals and H_2O_2 react with guanine residues in DNA and produce 8-hydroxydeoxyguanosine (8-OHdG). 8-OHdG serves as a biomarker for oxidative stress in various diseases.
Method: We investigated urinary 8-OHdG levels in 61 PD patients and 28 normal subjects to evaluate the correlation with various clinical features. We quantified disease severity using the Unified Parkinson's Disease Rating Scale for motor symptoms (UPDRS part 3), the Mini-Mental State Examination (MMSE) for mental function, and the Tottori University Hallucination Rating Scale (TUHARS) for quantifying hallucinations.
Results: There were significant correlations between 8-OHdG and all the examined parameters, but the partial correlation coefficients excluding contributions of all the other parameters showed that only TUHARS and UPDRS part 3 are significantly related to 8-OHdG. In particular, TUHARS correlates best with urinary 8-OHdG levels.
Conclusion: The significant correlation between urinary 8-OHdG levels and hallucinations but not with dementia suggests that hallucinations are likely to have unique but unidentified mechanisms that lead to excessive production of 8-OHdG.

1. Introduction

Molecular oxygen is used by the body to produce energy, but it in turn generates a large amount of reactive oxygen species (ROS). These species cause oxidative stress in cells even in the presence of a diverse array of defense mechanisms against ROS. Oxidative stress is causally associated with aging and various diseases. ROS including hydroxyl radicals and H_2O_2 react with guanine residues in DNA and produce 8-hydroxydeoxyguanosine (8-OHdG). The oxidized guanosine is misread as an adenine in DNA replication, and is elaborately repaired to prevent accumulation of G-to-A mutations. The excised 8-OHdG is excreted in urine, thereby serving as a key biomarker of oxidative DNA damage. This oxidized guanine (8-OHdG) is also a marker for susceptibility to cancer [1,2], diabetes mellitus [3], and neurodegenerative diseases including Alzheimer's disease [4] and Parkinson disease (PD) [5,6]. Indeed, several lines of evidence implicate increased oxidative stress in the pathogenesis of PD. In PD, 8-OHdG levels are increased selectively in the substantia nigra [7] and also in serum and cerebrospinal fluid [8,9].

The clinical pathology of PD involves both motor and non-motor dysfunction. Non-motor symptoms are increasingly recognized as significant causes of morbidity in late stage PD. It is also recognized that some patients with PD present with prodromal non-motor symptoms in the absence of motor symptoms. We measured urinary 8-OHdG levels in PD patients and examined which clinical scores best dictate the 8-OHdG levels. To our surprise, we found that degrees of hallucination best correlated with the urinary 8-OHdG levels.

2. Methods

The study protocol was approved by the Human Ethics Review Committee of the Nagoya University Graduate School of Medicine, and all PD patients and normal subjects gave their written informed consent to the investigation.

☆ The review of this paper was entirely handled by an Associate Editor, Eng-King Tan.

* Corresponding authors.
E-mail addresses: hirasan@med.nagoya-u.ac.jp (M. Hirayama), sobueg@med.nagoya-u.ac.jp (G. Sobue).

1353-8020/$ – see front matter © 2010 Elsevier Ltd. All rights reserved.
doi:10.1016/j.parkreldis.2010.11.004

We recruited 70 patients with PD (mean age ± SD, 65.6 ± 8.4 years; range, 42–81) and 50 normal controls (56.6 ± 11.7 years; range, 31–87). Patients were recruited from consecutive outpatients seen in the Department of Neurology, Nagoya University Hospital, from September though December 2009. Patients with probable idiopathic PD were diagnosed according to published criteria [10]. Smokers, patients with diabetes mellitus, brain infarction, who had undergone deep brain stimulation and obese patients and obese controls were excluded from our study because they have high urinary 8-OHdG levels [11]. We analyzed 61 PD patients and 38 controls. Their clinical features are shown in Table 1. The onset represents the first recognition of motor impairment. We quantified disease severity using the Unified Parkinson's Disease Rating Scale for motor symptoms (UPDRS part 3), the Mini-Mental State Examination (MMSE) for mental function, and the Tottori University Hallucination Rating Scale (TUHARS) for quantifying hallucinations [12]. We employed TUHARS, because, in UPDRS, hallucinations are scored only in item 2 of part 1. The Parkinson Psychosis Questionnaire (PPQ) is able to quantify visual hallucinations [13], but PPQ is not appropriate for use with Japanese patients. The total TUHARS score correlates well with the hallucinations/illusions score in the PPQ ($r = 0.965$, $P < 0.001$) [12]. Although Scales for Outcomes of Parkinson's disease-COG, Parkinson's-cognitive rating scale, and Mini-mental Parkinson and Parkinson neuropsychometric dementia assessment scales are specifically designed to quantify cognitive impairment of PD [14], these scales have not been well validated in Japanese patients. We thus employed MMSE to estimate cognitive impairment.

Urine samples were obtained from each individual in the morning (9–12 AM) and immediately stored at −20 °C. We instructed the patients and controls to avoid physical activity in the 24 h before providing the sample. Urinary 8-OHdG concentrations were measured using an ELISA with a monoclonal antibody specific for 8-OHdG. Urinary 8-OHdG and creatinine (Cr) levels were anonymously measured by the Mitsubishi Chemical Medience Co. (Tokyo, Japan) [15]. Urinary 8-OHdG levels were normalized by urinary Cr levels to adjust for urine volumes.

As dopamine agonists reportedly induce hallucinations [16]. Dopamine agonists had already been discontinued in hallucinating PD patients before entry to this study, whereas non-hallucinating patients tended to be taking dopamine agonists. To avoid biases imposed by therapeutic interventions, we excluded dosage of dopamine agonists from our analysis.

Quantitative data are presented as means ± SD. We employed Student's *t*-test, Pearson's correlation coefficient, and multivariate analysis using the statistical package JMP8 (SAS Institute, Carry, NC). For the correlation analysis, *P* values less than 0.05 and correlation coefficients greater than 0.4 were considered to be significant. As clinical parameters are all related each other [5,6], we reanalyzed partial correlations to exclude contributions of all the other parameters.

3. Results

We observed a moderate correlation ($r = 0.35$, $P < 0.05$) between urinary 8-OHdG excretion and aging in normal individuals. Among the 38 controls, we thus selected 28 subjects (65.7 ± 7.7 years, 18 males at 64.0 ± 7.1 years, 10 females at 68.8 ± 9.1 years) of a minimum age of 55 years to match the ages of PD patients. Our cohort of 61 PD patients comprised 29 males (65.1 ± 8.6 years) and 32 females (65.1 ± 8.0 years) with a mean age of 65.1 ± 8.3 years. Urinary 8-OHdG levels ranged from 5.4 to 12.0 ng/mg Cr (mean 8.8 ± 1.6) in the 28 controls, and 4.8 to 23.8 ng/mg Cr (mean 10.7 ± 4.0) in the 61 PD patients ($P < 0.01$). Urinary 8-OHdG levels were not significantly different between males and females in both controls (males, 8.6 ± 1.8 ng/mg Cr; females, 8.1 ± 2.1) and PD patients (males, 10.2 ± 3.6; females, 11.3 ± 4.3).

Table 1
Clinical features of 61 PD patients.

Clinical features	Mean ± SD	Range
Age at examination (years)	65.1 ± 8.3	42–81
Duration from onset (years)	7.7 ± 6.1	1–23
Age at onset (years)	56.8 ± 8.7	39–73
Yahr	2.8 ± 1.1	1–5
UPDRS part 1	3.3 ± 3.2	0–13
UPDRS part 2	11.8 ± 10.0	0–49
UPDRS part 3	22.9 ± 16.9	1–87
TUHARS	4.24 ± 6.1	0–24
MMSE	28.4 ± 2.8	18–30
Levodopa dose (mg/day)	309 ± 216	0–1200

We assumed that the normal urinary 8-OHdG levels were no more than 12 ng/mg Cr (mean + 2SD of 28 controls). We thus divided 61 PD patients into two groups with high (>12 ng/mg Cr, 17patients) and normal (≤12 ng/mg Cr, 44 patients) 8-OHdG levels. We found that the age at time of study, the disease duration, UPDRS part 3, TUHARS, MMSE and the levodopa dose were significantly higher in the high 8-OHdG group (Table 2). Similarly, we also found that the 8-OHdG levels demonstrate significant correlations with the age at examination, the disease duration, UPDRS part 3, TUHARS, MMSE, and the levodopa dose (Table 3). Among these, TUHARS showed the highest correlation coefficient. As the clinical parameters are mutually related each other, we calculated partial correlation coefficients (r') to exclude contributions of other parameters and to delineate contribution of each parameter to the 8-OHdG levels. The partial correlation analysis revealed that the age at time of study, the disease duration, MMSE, and the levodopa dose were not significantly related to the 8-OHdG levels, while TUHARS and UPDRS part 3 were significantly related to 8-OHdG (Table 3). As the r' value of TUHARS remained high after excluding effects of the other parameters, we plotted 8-OHdG against TUHARS and found that 40 out of 41 patients without hallucinations (98%) fell in the range of the mean ± 2SD of normal controls (5.6–12.0 ng/mg Cr) (Fig. 1).

4. Discussion

PD has been recognized as a movement disorder presenting with various motor symptoms, but there has been a gradual realization that PD is also associated with a broad spectrum of non-motor symptoms. These include anhedonia, depression, cognitive dysfunction, hallucinations, and complex behavioral disorders. Sato and colleagues previously reported that urinary 8-OHdG levels correlate to Hoehn and Yahr staging [5]. In this study, we quantified additional clinical features of PD, and found that urinary 8-OHdG levels correlate with all the examined clinical parameters except for age at onset. Among these, urinary 8-OHdG correlates most with hallucinations, yielding the correlation coefficient of 0.857 and the partial correlation coefficient of 0.761. Alam and colleagues reported increased 8-OHdG in the substantia nigra in PD [7]. Sato and colleagues postulated that high urinary 8-OHdG levels are possibly due to mitochondrial dysfunction in skeletal muscles because the substantia nigra is too small to generate a discernible amount of 8-OHdG [5]. Although our observations do not negate previous studies, urinary 8-OHdG is more likely to arise from dysfunction of neuronal cells and circuits that culminate in hallucinations. Hallucinations reportedly occur in 50% of patients with PD [17] and have a persistent and progressive nature [16]. Hallucinations experienced by PD patients have been postulated to occur via the following mechanisms: dopaminergic over-activity in the limbic system and cerebral cortices [18]; an imbalance with cholinergic neurotransmission [19]; dysfunction of the frontal areas associated with the control of attention [20]; PD-associated retinopathy [21]; decline of both image recognition speed and sustained attention

Table 2
Differences in clinical features between high and low urinary 8-OHdG levels in PD.

Clinical parameter	High level $N = 17$	Normal level $N = 44$	*P* value
Age at onset	56.5 ± 8.7	56.9 ± 8.8	n.s.
Age at exam	69.7 ± 7.5	63.3 ± 6.3	$P < 0.01$
Duration	12.5 ± 7.5	5.9 ± 4.3	$P < 0.001$
UPDRS part 3	35.8 ± 19.1	17.7 ± 12.6	$P < 0.0001$
TUHARS	12.6 ± 4.5	1.0 ± 2.3	$P < 0.0001$
MMSE	26.5 ± 4.2	29.1 ± 1.6	$P < 0.01$
Levodopa dose	441 ± 212	257 ± 197	$P < 0.01$

Table 3
Correlation coefficients (r) and partial correlation coefficients (r') normalized for all the other factors between 8-OHdG and the indicated clinical parameters.

Clinical parameter	r	P value	r'	P value
Age at exam	0.336	<0.05	0.062	n.s.
Duration	0.594	<0.0001	0.021	n.s.
UPDRS part 3	0.615	<0.0001	0.275	<0.05
TUHARS	0.857	<0.0001	0.761	<0.0001
MMSE	−0.499	<0.0001	−0.213	n.s.
Levodopa dose	0.522	<0.0001	0.122	n.s.

n.s., not significant.

[22]; alterations of brainstem sleep-wake and dream regulation [23]. Hallucinations are also associated with myocardial sympathetic dysfunction in PD [24]. Dysregulation of β1-adrenergic system in PD tends to cause myocardial tachycardia [25], which may increase the myocardial oxidative stress. In addition hallucinating patients show significantly lower cerebral blood flow in temporal regions, the inferior parietal lobule, precuneus gyrus, and occipital cortex than non-hallucinating patients [26,27], which may increase cerebral oxidative stress. Motor dysfunctions are mostly due to degeneration of the substantia nigra and related structures, whereas hallucinations are likely to represent more extensive impairment of cerebral nuclei and cortices. The difference in the number of affected neurons may explain why increased urinary 8-OHdG levels correlated more with hallucinations than motor symptoms. Although PD patients with hallucinations frequently develop dementia and show widespread atrophy involving limbic, paralimbic, and neocortical areas [28], the partial correlation coefficient between 8-OHdG and MMSE was lower than TUHARS in our patients. This also suggests that the number of affected neurons alone does not simply account for the increased urinary 8-OHdG levels. Hallucinations should represent neuronal hyperactivity, whereas dementia is caused by loss of neuronal activities. The difference in the ways the neurons are affected may explain why 8-OHdG correlates with hallucinations but not with dementia.

The MMSE inevitably has floor effects in subjects with severe cognitive impairment and ceiling effects in subjects with mild cognitive impairment in PD [14], however, other cognitive impairment scales that are specifically designed for PD have not been well validated in Japanese patients with PD. Further studies are required to estimate the correlation between 8-OHdG and PD-specific cognitive impairments.

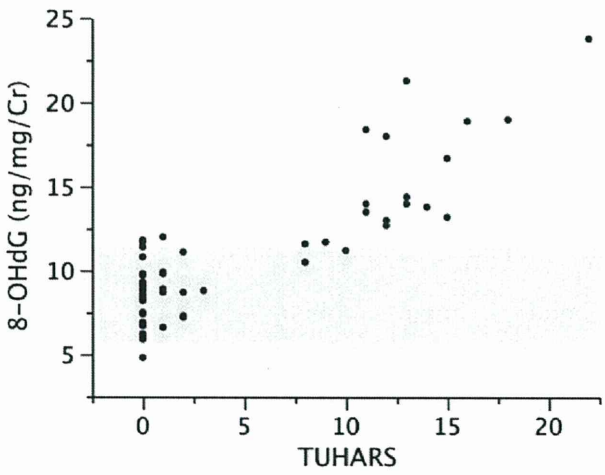

Fig. 1. Urinary 8-OHdG levels are plotted against TUHARS scores. Shaded area indicates the mean ± 2SD of 8-OHdG in age-matched controls.

In our studies, we only quantified degrees of hallucinations and cognitive impairments. PD is also associated with a broad spectrum of non-motor symptoms including sleepiness, depression, autonomic dysfunctions, and complex behavioral disorders. Quantification of other non-motor symptoms is required to conclude if other factors are also associated with elevated urinary 8-OHdG levels.

Financial disclosure

None of the authors have any financial disclosures.

Competing interests

None.

Acknowledgements

This work was supported by Grants-in-Aid from the Ministry of Education, Culture, Sports, Science, and Technology of Japan, and the Ministry of Health, Labor, and Welfare of Japan.

References

[1] Erhola M, Toyokuni S, Okada K, Tanaka T, Hiai H, Ochi H, et al. Biomarker evidence of DNA oxidation in lung cancer patients: association of urinary 8-hydroxy-2′-deoxyguanosine excretion with radiotherapy, chemotherapy, and response to treatment. FEBS Lett 1997;409:287–91.
[2] Halliwell B, Zhao K, Whiteman M. The gastrointestinal tract: a major site of antioxidant action? Free Radic Res 2000;33:819–30.
[3] Leinonen J, Lehtimaki T, Toyokuni S, Okada K, Tanaka T, Hiai H, et al. New biomarker evidence of oxidative DNA damage in patients with non-insulin-dependent diabetes mellitus. FEBS Lett 1997;417:150–2.
[4] Mecocci P, Polidori MC, Ingegni T, Cherubini A, Chionne F, Cecchetti R, et al. Oxidative damage to DNA in lymphocytes from AD patients. Neurology 1998;51:1014–7.
[5] Sato S, Mizuno Y, Hattori N. Urinary 8-hydroxydeoxyguanosine levels as a biomarker for progression of Parkinson disease. Neurology 2005;64:1081–3.
[6] Chen CM, Liu JL, Wu YR, Chen YC, Cheng HS, Cheng ML, et al. Increased oxidative damage in peripheral blood correlates with severity of Parkinson's disease. Neurobiol Dis 2009;33:429–35.
[7] Alam ZI, Jenner A, Daniel SE, Lees AJ, Cairns N, Marsden CD, et al. Oxidative DNA damage in the parkinsonian brain: an apparent selective increase in 8-hydroxyguanine levels in substantia nigra. J Neurochem 1997;69:1196–203.
[8] Kikuchi A, Takeda A, Onodera H, Kimpara T, Hisanaga K, Sato N, et al. Systemic increase of oxidative nucleic acid damage in Parkinson's disease and multiple system atrophy. Neurobiol Dis 2002;9:244–8.
[9] Gmitterova K, Heinemann U, Gawinecka J, Varges D, Ciesielczyk B, Valkovic P, et al. 8-OHdG in cerebrospinal fluid as a marker of oxidative stress in various neurodegenerative diseases. Neurodegener Dis 2009;6:263–9.
[10] Gelb DJ, Oliver E, Gilman S. Diagnostic criteria for Parkinson disease. Arch Neurol 1999;56:33–9.
[11] van Zeeland AA, de Groot AJ, Hall J, Donato F. 8-Hydroxydeoxyguanosine in DNA from leukocytes of healthy adults: relationship with cigarette smoking, environmental tobacco smoke, alcohol and coffee consumption. Mutat Res 1999;439:249–57.
[12] Wada-Isoe K, Ohta K, Imamura K, Kitayama M, Nomura T, Yasui K, et al. Assessment of hallucinations in Parkinson's disease using a novel scale. Acta Neurol Scand 2008;117:35–40.
[13] Dubois B, Burn D, Goetz C, Aarsland D, Brown RG, Broe GA, et al. Diagnostic procedures for Parkinson's disease dementia: recommendations from the movement disorder society task force. Mov Disord 2007;22:2314–24.
[14] Kulisevsky J, Pagonabarraga J. Cognitive impairment in Parkinson's disease: tools for diagnosis and assessment. Mov Disord 2009;24:1103–10.
[15] Omata N, Tsukahara H, Ito S, Ohshima Y, Yasutomi M, Yamada A, et al. Increased oxidative stress in childhood atopic dermatitis. Life Sci 2001;69:223–8.
[16] Goetz CG, Leurgans S, Pappert EJ, Raman R, Stemer AB. Prospective longitudinal assessment of hallucinations in Parkinson's disease. Neurology 2001;57:2078–82.
[17] Williams DR, Lees AJ. Visual hallucinations in the diagnosis of idiopathic Parkinson's disease: a retrospective autopsy study. Lancet Neurol 2005;4:605–10.
[18] Wolters EC, Francot CM. Mental dysfunction in Parkinson's disease. Parkinsonism Relat Disord 1998;4:107–12.
[19] Manganelli F, Vitale C, Santangelo G, Pisciotta C, Iodice R, Cozzolino A, et al. Functional involvement of central cholinergic circuits and visual hallucinations in Parkinson's disease. Brain 2009;132:2350–5.
[20] Ramirez-Ruiz B, Marti MJ, Tolosa E, Falcon C, Bargallo N, Valldeoriola F, et al. Brain response to complex visual stimuli in Parkinson's patients with

hallucinations: a functional magnetic resonance imaging study. Mov Disord 2008;23:2335–43.
[21] Devos D, Tir M, Maurage CA, Waucquier N, Defebvre L, Defoort-Dhellemmes S, et al. ERG and anatomical abnormalities suggesting retinopathy in dementia with Lewy bodies. Neurology 2005;65:1107–10.
[22] Meppelink AM, Koerts J, Borg M, Leenders KL, van Laar T. Visual object recognition and attention in Parkinson's disease patients with visual hallucinations. Mov Disord 2008;23:1906–12.
[23] Kulisevsky J, Roldan E. Hallucinations and sleep disturbances in Parkinson's disease. Neurology 2004;63:S28–30.
[24] Kitayama M, Wada-Isoe K, Irizawa Y, Nakashima K. Association of visual hallucinations with reduction of MIBG cardiac uptake in Parkinson's disease. J Neurol Sci 2008;264:22–6.
[25] Nakamura T, Hirayama M, Ito H, Takamori M, Hamada K, Takeuchi S, et al. Dobutamine stress test unmasks cardiac sympathetic denervation in Parkinson's disease. J Neurol Sci 2007;263:133–8.
[26] Okada K, Suyama N, Oguro H, Yamaguchi S, Kobayashi S. Medication-induced hallucination and cerebral blood flow in Parkinson's disease. J Neurol 1999; 246:365–8.
[27] Matsui H, Nishinaka K, Oda M, Hara N, Komatsu K, Kubori T, et al. Hypoperfusion of the visual pathway in parkinsonian patients with visual hallucinations. Mov Disord 2006;21:2140–4.
[28] Ibarretxe-Bilbao N, Ramirez-Ruiz B, Junque C, Marti MJ, Valldeoriola F, Bargallo N, et al. Differential progression of brain atrophy in Parkinson's disease with and without visual hallucinations. J Neurol Neurosurg Psychiatr 2010;81:650–7.

4396–4404 *Nucleic Acids Research, 2011, Vol. 39, No. 10* *Published online 2 February 2011*
doi:10.1093/nar/gkr026

AG-dependent 3′-splice sites are predisposed to aberrant splicing due to a mutation at the first nucleotide of an exon

Yuan Fu, Akio Masuda, Mikako Ito, Jun Shinmi and Kinji Ohno*

Division of Neurogenetics, Center for Neurological Diseases and Cancer, Nagoya University Graduate School of Medicine, 65 Tsurumai, Showa-ku, Nagoya 466-8550, Japan

Received October 10, 2010; Revised December 23, 2010; Accepted January 12, 2011

ABSTRACT

In pre-mRNA splicing, a conserved AG/G at the 3′-splice site is recognized by U2AF^{35}. A disease-causing mutation abrogating the G nucleotide at the first position of an exon (E^{+1}) causes exon skipping in *GH1*, *FECH* and *EYA1*, but not in *LPL* or *HEXA*. Knockdown of U2AF^{35} enhanced exon skipping in *GH1* and *FECH*. RNA-EMSA revealed that wild-type *FECH* requires U2AF^{35} but wild-type *LPL* does not. A series of artificial mutations in the polypyrimidine tracts of *GH1*, *FECH*, *EYA1*, *LPL* and *HEXA* disclosed that a stretch of at least 10–15 pyrimidines is required to ensure normal splicing in the presence of a mutation at E^{+1}. Analysis of nine other disease-causing mutations at E^{+1} detected five splicing mutations. Our studies suggest that a mutation at the AG-dependent 3′-splice site that requires U2AF^{35} for spliceosome assembly causes exon skipping, whereas one at the AG-independent 3′-splice site that does not require U2AF^{35} gives rise to normal splicing. The AG-dependence of the 3′-splice site that we analyzed in disease-causing mutations at E^{+1} potentially helps identify yet unrecognized splicing mutations at E^{+1}.

INTRODUCTION

In higher eukaryotes, generation of functional mRNA is dependent on the removal of introns from pre-mRNA by splicing (1). The splicing process occurs in the spliceosome, the major components of which include five small nuclear RNAs and their associated proteins (U1, U2, U4, U5 and U6 snRNPs) in addition to a large number of non-snRNP proteins (2). In the first step of assembly of the spliceosome, U1 snRNP, SF1, U2AF^{65} and U2AF^{35} bind to the splicing *cis*-elements at the 5′ splice site (ss), the branch point sequence (BPS), the polypyrimidine tract (PPT) and the acceptor site, respectively, to form complex E (3).

Yeast has a well conserved BPS of UACUAAC (4), whereas we recently reported that human carries a highly degenerate BPS of yUnAy, where '*y*' and '*n*' represent pyrimidines and any nucleotides, respectively (5). Degeneracy of the human BPS supports a notion that the human BPS is likely to be recognized along with the downstream PPT where U2AF^{65} binds and possibly with the invariant AG dinucleotide at the 3′ ss where U2AF^{35} binds (6,7). U2AF^{65} and U2AF^{35} also make a heterodimer (8). In PPT, uridines are preferred over cytidines (9,10). In addition, PPT with 11 continuous uridines is highly competent and the position of such PPT is not critical (10). On the other hand, PPTs with only five or six uridines are required to be located close the 3′ AG for efficient splicing. In addition, phosphorylated DEK binds to and cooperates with U2AF^{35} for proper recognition of the 3′ ss (11).

In the next step of the spliceosome assembly, the bound U2AF^{65} and U2AF^{35} facilitate substitution of SF1 for U2snRNP at the branch point to form complex A. Introns carrying a long stretch of PPT do not require U2AF^{35} for this substitution, which is called 'AG-independent 3′ ss' (12–15). On the other hand, introns with a short or degenerate PPT require both U2AF^{65} and U2AF^{35} for this substitution, which is called 'AG-dependent 3′ ss'. Thereafter, the U4/U6.U5 tri-snRNP is integrated into the spliceosome to form complex B and the initial assembly of the spliceosome is completed.

The invariant AG dinucleotides are frequently reported targets of mutations causing human diseases, and the most frequent consequence is skipping of one or more exons (16). In addition, even mutations in highly degenerate BPS (5) and PPT (17) give rise to aberrant splicing

*To whom correspondence should be addressed. Tel: +81 52 744 2446; Fax: +81 52 744 2449; Email: ohnok@med.nagoya-u.ac.jp